

Synchrotron radiation for beam diagnostics: Numerical calculations of the single electron spectrum

Oliver Grimm
University of Hamburg

June 18, 2008

Abstract

This paper presents a simple numerical algorithm to calculate single-electron synchrotron radiation spectra resulting from acceleration in an arbitrary magnetic field. The focus is on an exact implementation of the basic formula governing the emission, not on fast computation. Comparisons to several analytical calculations are made, and some results applicable for the FLASH free-electron laser are given.

1 Introduction

Synchrotron radiation has many applications in electron beam diagnostics. It allows measurements of the transverse and longitudinal structure of electron bunches, as well as the energy distribution. The radiation is emitted fully parasitically in dipole magnets that are present in circular as well as linear accelerators or storage rings. The wide spectral range that makes it desirable as a source in its own right also is attractive for beam diagnostics.

Especially for longitudinal electron beam diagnostics using coherent radiation techniques, a comprehensive understanding of the single-electron spectrum is required, as this is needed to unfold the measured spectra and to deduce or assess the longitudinal charge distribution [Gri06].¹ This report summarizes the basics of synchrotron radiation calculations, presents a simple code to numerically derive the single-electron spectrum, and gives several results applicable to the free-electron laser FLASH at DESY.

The typical synchrotron radiation pulse duration is of the order of picoseconds or less, a time-scale that usual (bolometric) radiation detectors cannot resolve. It is therefore not the instantaneous power that is relevant, but the energy within a pulse. Frequency is always given as cycle frequency, not angular frequency. The Fourier transform of a function is designated with the same symbol as the function itself, only distinguished by its variable. All calculations are done in SI units.

Sect. 2 presents the necessary background for the calculation of synchrotron radiation spectra and lists some analytical calculations. Sect. 3 then details the numerical algorithm and some basic results. Several calculations relevant explicitly for FLASH are summarized in Sect. 4. Additional theoretical material is collected in the appendices.

¹Note that the derivation in this report explicitly requires that each electron radiates the same electric field in time domain, only shifted according to its longitudinal position within the bunch. This is not always guaranteed if the magnetic field changes rapidly and the head of the bunch can be subject to varying fields from the tail [Sal97]. More elaborate numerical simulations than reported here are necessary under such circumstances, taking into account the self-interaction within the bunch.

Most explicit calculations presented will use the nominal parameters of a dipole of the first FLASH bunch compressor chicane: magnetic field 0.27 T, giving a bending radius of 1.6 m at 130 MeV. The effective length of such a dipole is 50 cm, resulting in a nominal deflection of 18°.

2 Single-electron spectrum: Basics and analytical calculations

2.1 General magnetic field

Synchrotron radiation is emitted by a relativistic electron accelerated transversely to its motion by passing a magnetic field. The starting point for the calculation of the emission spectrum resulting from an arbitrary magnetic field are the retarded Liénard-Wiechert potentials [Jack75]. They give the electric and magnetic field resulting from a general acceleration of an elementary charge at some observation point as²

$$\vec{E}(t) = \frac{e}{4\pi\epsilon_0} \frac{\vec{n}(t) - \vec{\beta}(t)}{\gamma^2(1 - \vec{\beta}(t) \cdot \vec{n}(t))^3 L^2(t)} \Big|_{\text{ret}} + \frac{e}{4\pi\epsilon_0 c} \frac{\vec{n}(t) \times ((\vec{n}(t) - \vec{\beta}(t)) \times \dot{\vec{\beta}}(t))}{(1 - \vec{\beta}(t) \cdot \vec{n}(t))^3 L(t)} \Big|_{\text{ret}} \quad (1a)$$

$$\vec{B}(t) = \frac{1}{c} \vec{n}(t)|_{\text{ret}} \times \vec{E}(t), \quad (1b)$$

where the velocity $\vec{\beta} = \vec{v}/c$, the acceleration $\dot{\vec{\beta}}$, the unit vector \vec{n} from the charge to the observation point, and the corresponding distance L all need to be evaluated at the retarded time $t' = t - L(t)/c$ to account for the finite propagation velocity. The first part of $\vec{E}(t)$ is usually called the velocity term, the second the acceleration term.

The power flow in time-domain follows from the Poynting vector $\vec{S}(t)$, given in free space by (see App. A.1)

$$\vec{S}(t) = \frac{1}{\mu_0} \vec{E}(t) \times \vec{B}(t) = \epsilon_0 c \left(|\vec{E}(t)|^2 \vec{n}(t)|_{\text{ret}} - (\vec{E}(t) \cdot \vec{n}(t)|_{\text{ret}}) \vec{E}(t) \right). \quad (2)$$

The relation of retarded time along the trajectory to observer time at point P can be calculated with reference to Fig. 1. For a small time difference $\Delta t' = t'_2 - t'_1$

$$\begin{aligned} L(t'_2) &= \sqrt{(-L(t'_1) + \Delta t' \beta c \cos \alpha(t'))^2 + (\Delta t' \beta c \sin \alpha(t'))^2} \\ &\approx L(t'_1) \left(1 - \frac{\Delta t' \beta c (1 - \frac{1}{2} \alpha(t')^2)}{L(t'_1)} \right), \end{aligned}$$

where the square root and the cosine are expanded to first non-trivial order.³ Now follows

$$\Delta t = t_2 - t_1 = t'_2 + \frac{L(t'_2)}{c} - t'_1 - \frac{L(t'_1)}{c} = \Delta t' + \frac{L(t'_2) - L(t'_1)}{c} = \Delta t' \left(1 - \beta + \frac{\beta}{2} \alpha(t')^2 \right).$$

Using the approximation $1 - \beta = 1/(2\gamma^2)$, valid for $\gamma \gg 1$, this can be expressed in differential form as

$$\frac{dt}{dt'} = \frac{1 + \alpha(t')^2 \gamma^2}{2\gamma^2}. \quad (3)$$

The dependence of the angle α on the trajectory in retarded time makes evaluation of this expression analytically often difficult.

²The designation for the observation point \vec{r} is suppressed in this report for brevity, i.e. $\vec{E}(t) \equiv \vec{E}(\vec{r}, t)$.

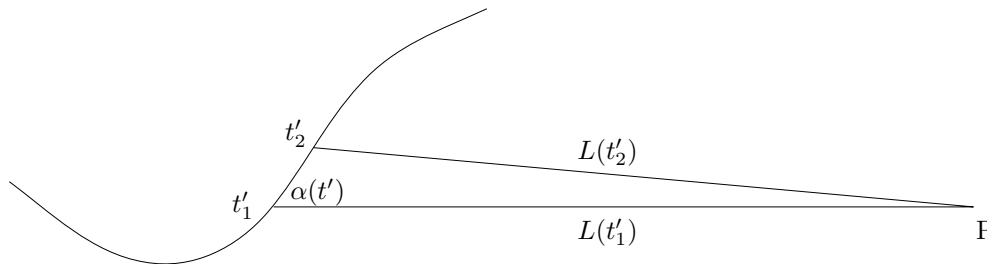


Figure 1 General trajectory to illustrate the relation between retarded and observer time.

At large distance from a source region, the second term on the right side of (2) is absent since then $\vec{E}(t)$ is perpendicular to $\vec{n}(t')$ due to the faster reduction of the first term in (1a) with distance than the second.

The frequency spectrum follows through application of a Fourier transformation,

$$\vec{E}(\nu) = \int_{-\infty}^{\infty} \vec{E}(t) e^{-2\pi i \nu t} dt, \quad (4)$$

giving the energy density spectrum in units of J/(Hz m²) at a given position at large distance as (see App. A)

$$\frac{d^2U}{d\nu dA} \approx 2\epsilon_0 c |\vec{E}(\nu)|^2. \quad (5)$$

It should be noted that the labeling of the acceleration term as 'radiation term', as is sometimes done, is not entirely correct, since some part of the radiated field energy contained in the velocity term at small distances ends up in the acceleration term at larger distance once the former has died out due to its stronger dependence on distance. A charge in uniform motion will carry of course only the velocity field along and does not lose energy. An accelerated charge will have a different behaviour of the velocity vector $\vec{\beta}$ and of the unit vector \vec{n} in the first term of (1a). The electric field contribution of this term is modified compared to the non-radiating case, thus contributing partly to the energy lost by the particle. Although at large distance all radiated power is accounted for by the acceleration term of (1a), part of that power appears in the velocity term at smaller distance. The velocity term does not only contain the static field.

2.2 Asymptotic expressions

The emitted radiation spectrum depends on the acceleration of the electron, which in turn is an effect of the magnetic field (see App. C). Clearly, no general solution for arbitrary magnetic fields can be given. However, several asymptotic expressions have been derived by various authors. These are useful not only for understanding the basic principles of synchrotron radiation generation, but also as benchmarks to test the performance and correct operation of numerical codes. Some of these asymptotic results will be briefly summarized in this section.

2.2.1 Synchrotron radiation from circular motion

Using the approximations

- Constant magnetic field: The particle follows a circular trajectory (radius R).

- Large distance of the observation point from the source region: \vec{n} and L are constant in time and only the acceleration term in (1a) is considered.
- Highly relativistic motion ($\gamma \gg 1$): The radiation is emitted in a narrow cone.

the angular spectral energy distribution of a single electron is calculated in [Jack75]:

$$\left(\frac{d^2U}{d\lambda d\Omega}\right)_{\text{c.m.}} = \frac{2e^2 R^2}{3\epsilon_0 \lambda^4} \left(\frac{1}{\gamma^2} + \Theta^2\right)^2 \left(K_{2/3}^2(\xi) + \frac{\Theta^2}{1/\gamma^2 + \Theta^2} K_{1/3}^2(\xi)\right), \quad (6)$$

where $\xi = \frac{2\pi R}{3\lambda} \left(\frac{1}{\gamma^2} + \Theta^2\right)^{3/2}$.

The first term in brackets refers to horizontal polarization (in the orbit plane), the second term to vertical polarization and Θ is the vertical observation angle. There is clearly no dependence on the horizontal angle for circular motion. Angle-integrating this yields

$$\left(\frac{dU}{d\lambda}\right)_{\text{c.m.}} = \frac{\sqrt{3}e^2 \gamma \lambda_c}{2\epsilon_0 \lambda^3} \int_{\lambda_c/\lambda}^{\infty} K_{5/3}(x) dx, \quad \text{where } \lambda_c = \frac{4\pi R}{3\gamma^3}. \quad (7)$$

K_α indicates a modified Bessel functions of order α .

The electric field in time domain for this case as observed in the plane of motion at 1 m distance is shown in Fig. 2. The acceleration term is symmetric with respect to $t = 0$ and the integral vanishes⁴, as can be seen from (1a), by evaluating (3) for circular motion. The calculation of the retarded time of the acceleration term zero crossings is straightforward from (1a). Considering a motion in the xy plane, $\vec{\beta}(t') = \beta(\cos(\beta ct'/R) \sin(\beta ct'/R) 0)$. For an observation point tangential to the trajectory at $t' = 0$, $\vec{n} = (1 \ 0 \ 0)$. The electric field in retarded time becomes zero if the nominator of the acceleration term vanishes. Expanding the cross product, this is the case if

$$\left(\vec{n} - \vec{\beta}(t')\right) \vec{n} \cdot \dot{\vec{\beta}}(t') - \dot{\vec{\beta}}(t') \left(1 - \vec{n} \cdot \vec{\beta}(t')\right) = 0.$$

The only component of this vector equation that does not vanish independent of t' is the y component, which yields

$$\cos \frac{\beta ct'}{R} = \beta,$$

and finally, after expansion of the cosine to first order and using $1 - \beta \approx 1/(2\gamma^2)$,

$$t' = \pm \frac{R}{\beta \gamma c}.$$

This corresponds to a trajectory angle of $\pm 1/\gamma$ with respect to the position at $t = 0$. With the help of (3), the corresponding duration in observer time can be calculated. Due to the circular trajectory, $\alpha(t') = \beta ct'/R$, so

$$t = \pm \int_0^{\frac{R}{\beta \gamma c}} \frac{1 + \alpha(t')^2 \gamma^2}{2\gamma^2} dt' = \pm \frac{2R}{3\gamma^3 c} = \pm \frac{\lambda_c}{2\pi c} = \pm \frac{1}{\omega_c}. \quad (8)$$

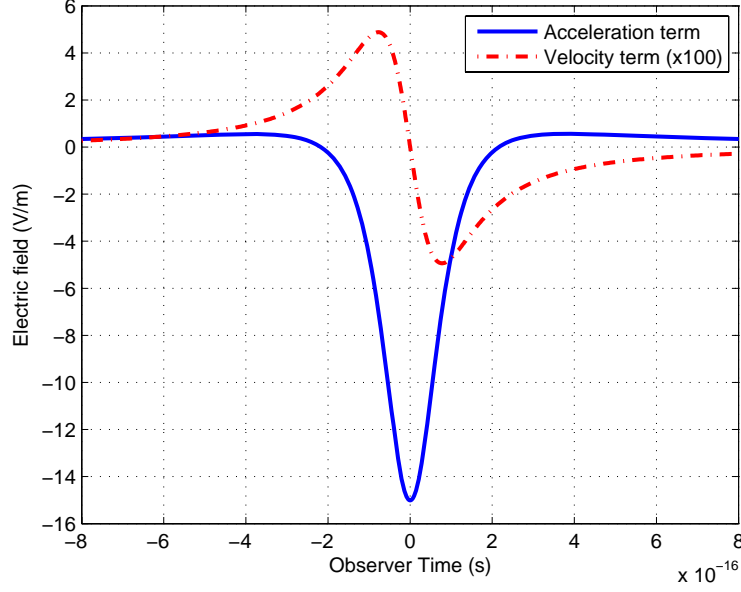


Figure 2 Electric field for the case of circular motion. The observation point is on the bending plane at 1 m distance tangentially, electron energy 130 MeV, bending radius 1.6 m. The weak field from the velocity term, shown multiplied by 100, is disregarded in the usual calculation of the radiation spectrum.

The electric field zero crossings occur thus at a time equal to the inverse of the critical angular frequency ω_c . For the parameters of a FLASH bunch compressor dipole, this yields $t = \pm 2.2 \times 10^{-16}$ s, as seen in Fig. 2.

The peak electric field in forward direction can also easily be deduced from (1a), using (18) and the fact that \vec{n} is parallel to the velocity and perpendicular to the acceleration at $t = 0$:

$$E(0) = \frac{-e^2}{\pi\epsilon_0 mc} \frac{\gamma^3 B}{L} = \frac{-e\gamma^4}{\pi\epsilon_0 LR}.$$

The emitted power during the motion along the circle is

$$P = \frac{e^2 c}{6\pi\epsilon_0} \frac{\gamma^4}{R^2}. \quad (9)$$

This expression remains valid as the instantaneous power in case the magnetic field and thus the radius changes. Integration over the trajectory will give the total energy lost by the particle.

For long wavelengths $\lambda \gg \lambda_c$, often of particular interest for coherent radiation diagnostics, (6) becomes for $\Theta = 0$

$$\left(\frac{d^2 U}{d\lambda d\Omega} \right)_{\text{l.w.}} = \frac{e^2}{2\epsilon_0} \left(\frac{\Gamma(2/3)}{\pi} \right)^2 \left(\frac{3}{4} \right)^{1/3} \frac{(2\pi R)^{2/3}}{\lambda^{8/3}},$$

which is independent of energy for a given radius of curvature. The typical opening angle in this case is

$$\Theta_{\text{l.w.}} = \frac{1}{\gamma} \left(\frac{\lambda}{\lambda_c} \right)^{1/3} = \left(\frac{3\lambda}{2\pi R} \right)^{1/3}, \quad (10)$$

⁴This is why the spectrum drops to zero at zero frequency, as $\vec{E}(\nu = 0) = \int_{-\infty}^{\infty} \vec{E}(t) dt$.

which is also independent of energy.

These formulae give the spectrum resulting from a single passage of the electron. Strictly, the integration in (4) runs from $-\infty$ to ∞ , and for circular motion a line spectrum results, consisting of harmonics of the revolution frequency. This can be seen by writing for $2m$ revolutions of period t_0 , where m is a positive integer,

$$\begin{aligned}\vec{E}_{2m}(\nu) &= \int_{-mt_0}^{mt_0} \vec{E}(t) e^{-2\pi i \nu t} dt = \sum_{k=-m}^m \int_{kt_0}^{(k+1)t_0} \vec{E}(t) e^{-2\pi i \nu t} dt \\ &= \sum_{k=-m}^m \int_0^{t_0} \vec{E}(t + kt_0) e^{-2\pi i \nu (t+kt_0)} dt = \sum_{k=-m}^m e^{-2\pi i \nu kt_0} \int_0^{t_0} \vec{E}(t) e^{-2\pi i \nu t} dt \\ &= \left(2 \sum_{k=1}^m \cos(2\pi \nu kt_0) + 1 \right) \int_0^{t_0} \vec{E}(t) e^{-2\pi i \nu t} dt,\end{aligned}$$

The relation $\vec{E}(t + kt_0) = \vec{E}(t)$ for any integer k is used. The emitted energy will be infinite for an infinite number of revolutions, therefore the power frequency spectrum is a more appropriate quantity:

$$I_{2m}(\nu) = \frac{2\epsilon_0 c |\vec{E}_{2m}(\nu)|^2}{(2m+1)t_0} = (2m+1)I_0(\nu) \left(\frac{2 \sum_{k=1}^m \cos(2\pi \nu kt_0) + 1}{2m+1} \right)^2.$$

$I_0(\nu)$ is the averaged power spectrum from a single passage. The term in brackets represents a line spectrum at integer multiples of $1/t_0$, with unit amplitude, and a line width decreasing with increasing m . The envelope of the spectrum remains the same as for a single passage, but the power is concentrated into progressively narrower frequency spikes.

2.2.2 Low-frequency radiation

In [Méot99], the low-frequency limit of the synchrotron radiation spectrum for a constant magnetic field of finite extend is calculated by neglecting the exponential term in (4) altogether and using only the acceleration term in (1a):

$$\vec{E}(\nu) = \int_{\Delta t} \vec{E}(t) dt.$$

Clearly, this is frequency independent. The validity requirement $\nu \Delta t \ll 1$, where Δt is the duration of the radiation pulse, can be expressed using the length of the magnetic field region L and the (typical) curvature radius ρ as

$$\nu \ll \frac{\gamma^2 c}{\pi L \left(1 + \frac{\gamma^2 L^2}{12\rho^2} \right)}.$$

For the parameters of a bunch compressor dipole, this yields $\nu \ll 150$ GHz, so that the validity is confined to wavelengths were the chamber cut-off (to be discussed below) already completely suppresses the spectrum. Except for benchmarking, this approximation is of no further use for application at FLASH.

2.2.3 Short magnet radiation

The far-field radiation spectrum for a weak magnet has been calculated analytically in [Coï79]. The main steps of the derivation are outlined here.

The acceleration of an electron by a magnetic field of constant direction, $\vec{B}_m(t) = B_m(t)\vec{n}_m$, is, from (18),

$$\dot{\vec{\beta}}(t) = \frac{eB_m(t)}{m\gamma} \vec{\beta}(t) \times \vec{n}_m.$$

The subscript m is used to clearly distinguish this static field from the emitted magnetic field (1b). The time-dependence of $\vec{B}_m(t)$ results from the movement of the electron through the spatially varying field. Neglecting now all time dependences in (1a) except that of the magnetic field magnitude which enters via the acceleration, and considering only the acceleration term, the electric field in time-domain can be written as

$$\vec{E}(t) = \frac{e^2}{4\pi\epsilon_0 mc} \frac{\vec{n} \times \left\{ \left(\vec{n} - \vec{\beta} \right) \times \left(\vec{\beta} \times \vec{n}_m \right) \right\}}{\gamma(1 - \vec{\beta} \cdot \vec{n})^3 L} B_m(t)|_{\text{ret}}.$$

The disregard of the time dependence of \vec{n} and L along with the velocity term implies a large distance of the observation point to the magnetic field region. The disregard of the time dependence of $\vec{\beta}$ additionally requires that the angle of the trajectory is changed much less than $1/\gamma$, which is the case for a short or weak magnet. With this condition (3) can be evaluated easily, as then α is constant, and so the compression between retarded and observer time is also constant: $dt/dt' = t/t'$. Now

$$\int_{-\infty}^{\infty} B_m(t)|_{\text{ret}} e^{-2\pi i\nu t} dt = \frac{1 + \alpha^2\gamma^2}{2\gamma^2} \int_{-\infty}^{\infty} B_m(t') e^{-2\pi i\nu \frac{1+\alpha^2\gamma^2}{2\gamma^2} t'} dt',$$

and the Fourier transform of $\vec{E}(t)$ can thus be written as

$$\vec{E}(\nu) = \frac{e^2}{\pi\epsilon_0 mc L} \frac{\gamma^3}{(1 + \alpha^2\gamma^2)^2} \vec{n} \times \left\{ \left(\vec{n} - \vec{\beta} \right) \times \left(\vec{\beta} \times \vec{n}_m \right) \right\} \int_{-\infty}^{\infty} B_m(t') e^{-2\pi i\nu \frac{1+\alpha^2\gamma^2}{2\gamma^2} t'} dt'.$$

This requires only an integration along the particle trajectory. The double cross product can be simplified according to

$$\begin{aligned} \vec{n} \times \left\{ \left(\vec{n} - \vec{\beta} \right) \times \left(\vec{\beta} \times \vec{n}_m \right) \right\} &= \vec{n} \times \left\{ \vec{\beta}(\vec{n} \cdot \vec{n}_m) - \vec{n}_m(\vec{n} \cdot \vec{\beta}) - \vec{\beta}(\vec{\beta} \cdot \vec{n}_m) + \vec{n}_m\beta^2 \right\} \\ &= \vec{n} \times \left\{ \vec{\beta}(\vec{n} \cdot \vec{n}_m) - \vec{n}_m(\cos\alpha - \beta^2) \right\} \\ &= \vec{n} \times \vec{\beta}(\vec{n} \cdot \vec{n}_m) - \vec{n} \times \vec{n}_m \left(\frac{1}{\gamma^2} - \frac{\alpha^2}{2} \right). \end{aligned}$$

The assumption has been made that the velocity is perpendicular to the magnetic field.

The requirement of a small change in trajectory direction is often not desirable for beam diagnostics purposes, as it will complicate outcoupling of the radiation that will almost co-propagate with the electron beam. A mirror with a small hole can be used that however needs to be inside of the ultra-high machine vacuum. A small aperture can have a significant effect on beam dynamics through wake fields.

2.2.4 Edge radiation

Of significant practical importance for beam diagnostics is radiation emitted by an electron traversing a region of non-constant magnetic field. Calculations of the long-wavelength component for the rising or falling edge of a dipole magnet, sometimes called edge radiation, are undertaken in [Chu93]. In the limit $\lambda \gg \lambda_c$, λ_c defined in (7), and for a magnetic field changing sufficiently fast, they find the expression

$$\left(\frac{d^2U}{d\lambda d\Omega}\right)_{\text{e.r.}} = \frac{e^2\gamma^2}{2\pi^2\epsilon_0\lambda^2} \left(\frac{\gamma^2\Phi^2}{(1+\gamma^2\Theta^2+\gamma^2\Phi^2)^2} + \frac{2c_1p^{1/3}\gamma\Phi}{1+\gamma^2\Theta^2+\gamma^2\Phi^2} + (c_1+c_2)p^{2/3} + \frac{\gamma^2\Theta^2}{(1+\gamma^2\Theta^2+\gamma^2\Phi^2)^2} - \frac{2c_3p^{2/3}\gamma^2\Theta^2}{1+\gamma^2\Theta^2+\gamma^2\Phi^2} \right), \quad (11)$$

$$\text{where } p = \frac{3\lambda_c}{4\lambda}, \quad c_1 = \frac{\pi}{3^{1/3}\Gamma(1/3)}, \quad c_2 = \frac{\pi}{3^{5/6}\Gamma(1/3)}, \quad c_3 = \frac{\pi}{3^{7/6}\Gamma(1/3)}.$$

There is only a weak frequency dependence through the low powers of p (as $d\lambda = \frac{\lambda^2}{c}d\nu$). Γ denotes the Gamma function, Φ the horizontal observation angle (in the bending plane), Θ the vertical angle. The first three terms in the large bracket refer to horizontal polarization, the last two to vertical polarization. If the typical distance scale over which the magnetic field changes is Δs , the condition of sufficiently fast changing can be formulated as

$$\Delta s \ll \lambda\gamma^2 \quad \text{or, if this is not fulfilled,} \quad \Delta s \ll \sqrt[3]{\lambda R^2} = \sqrt[3]{\lambda \left(\frac{3\lambda_c}{4\pi}\right)^2 \gamma^2},$$

where R is the bending radius once the magnetic field is constant. For a bunch compressor dipole, the typical scale for the rise and fall of the field is about 5 cm, the bending radius is 1.6 m at 130 MeV, so (11) is valid for $\lambda \gg 50 \mu\text{m}$ (second condition).

When the radiation spectrum is dominated by the edge effect, the possibility of interference from an edge of a preceding or following magnet must be considered, as will be seen in the numerical simulations below.

3 Numerical calculations

3.1 Principle of the numerical calculations

Fully general calculations can only be done numerically and are practically important, as usually none of the approximations hold to a sufficient degree. A numerical simulation will automatically include effects from the rise and fall of the magnetic field at the entrance and exit of the magnet (edge effect), the finite length of the field and possible interference from a previous or following magnet. Also shielding effects from the vacuum chamber can be included easily to a certain degree using mirror charges, see Sect. 3.8.

The numerical simulation is implemented in a straightforward manner, see the flow chart in Fig. 3. The essential parts of the Matlab implementation are listed in App. D.

1. An electron is tracked through the known magnetic fields with a given step size. The electric field strength at a given observation position at the future, advanced time given by the current distance is calculated using (1a), see Fig. 4. Depending on the rate of change of the field in observer time, the tracking step size is adapted. This approach avoids calculation of a retarded time, and allows to evaluate (3) easily.

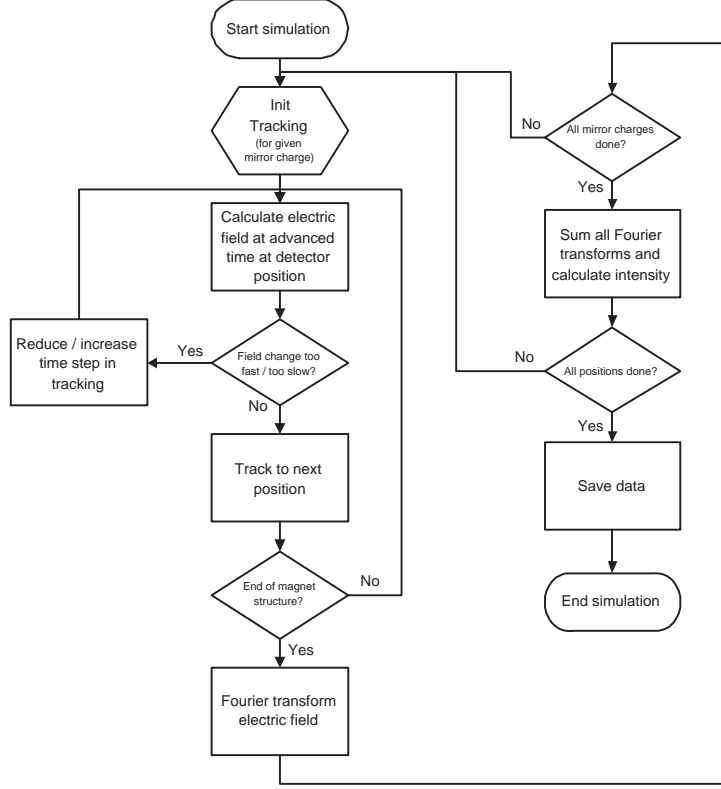


Figure 3 Flow chart of the numerical field simulation.

2. The time dependent electric field at the observer position is Fourier transformed.
3. The energy density spectrum $d^2U/(d\nu dA)$ is calculated from (5) or, in general, from (15).

To check if the result is numerically stable, the simulation is repeated with half the step size. This should result in only very small modifications. Even if this is the case, however, it is still important to be aware of the possibility of limited numerical precision from the particular software used.

The discrete Fourier transform is calculated as follows.

$$\begin{aligned}
 \vec{E}_0(\nu_j) &= \int_{-\infty}^{\infty} \vec{E}(t) e^{-2\pi i \nu_j t} dt = \sum_i \int_{t_i}^{t_{i+1}} \vec{E}(t) e^{-2\pi i \nu_j t} dt \approx \sum_i \vec{E}(t_i) \int_{t_i}^{t_{i+1}} e^{-2\pi i \nu_j t} dt \\
 &= \frac{1}{2\pi i \nu_j} \sum_i \vec{E}(t_i) (e^{-2\pi i \nu_j t_i} - e^{-2\pi i \nu_j t_{i+1}}) \\
 &= \frac{1}{2\pi i \nu_j} \sum_i \vec{E}(t_i) (e^{-2\pi i \nu_j t_i} - e^{-2\pi i \nu_j (t_i + \Delta t_i)}) \\
 &= \frac{1}{2\pi i \nu_j} \sum_i \vec{E}(t_i) e^{-2\pi i \nu_j t_i} (1 - e^{-2\pi i \nu_j \Delta t_i})
 \end{aligned} \tag{12}$$

The approximation is good as long as $\vec{E}(t)$ does not vary too much between adjacent times. Here, the index of $\vec{E}_0(\nu_j)$ refers to the zeroth order approximation, i.e. $\vec{E}(t)$ is assumed to be constant between two time steps. In App.B the formula for the first order is calculated. Compared to

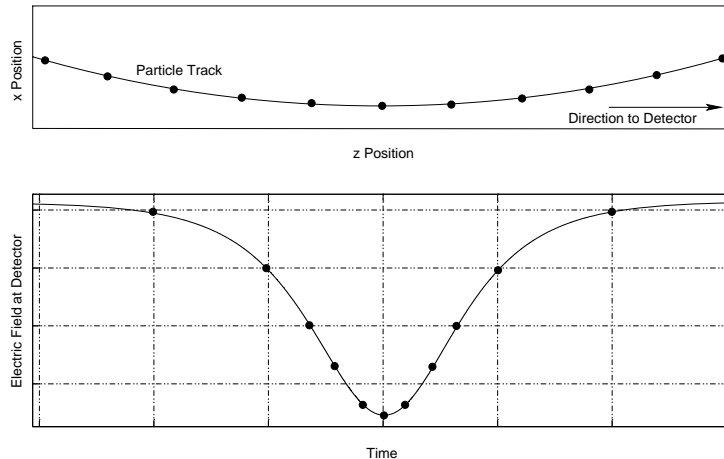


Figure 4 Equidistant tracking steps naturally result in non-equidistant spacing of the electric field during its peak due to the time compression from (3).

the implementation of (fast) Fourier transforms, this direct approach has the advantage of not requiring equidistant time steps.⁵

An option is to use directly an expression for the electric field in frequency domain, for example using a paraxial approximation for rapid computation [Gel05].

3.2 Comparison with analytic results

To check the correct behaviour of the numerical algorithm, its results for two of the analytically solved cases are presented in this section. The general parameters for the following calculations are, as usual, those of a dipole from the first bunch compressor of FLASH.

3.2.1 Circular motion

Results for circular motion are compared in Fig. 5 with the frequency spectrum (6) for two angles, $\Theta=0$ and $\Theta=1/\gamma$, and in Fig. 6 with the angular dependence. The agreement is very good, being limited at low frequencies by the simulation time (the minimum frequency that can be simulated is about the inverse of the simulation time, $2.3 \cdot 10^9$ Hz in this case) and at high frequencies by the size of the time steps.

3.2.2 Long-wavelength edge radiation

The transverse intensity distribution at 30 mm wavelength along the incoming beam direction at 10 m distance as calculated numerically is shown in Fig. 7 together with an analytic calculation using (11). The required condition for the validity of the analytic formula is fulfilled, and indeed there is a very good agreement between the two distributions. At such long wavelengths, the edge effect dominates the emitted radiation characteristic. The deflection of the beam for the assumed field polarity is towards negative horizontal offsets.

The transverse distributions are indeed very similar, as can be seen in the vertically integrated profiles of the horizontal polarization component shown in Fig. 8.

⁵To use an FFT algorithm, it would be necessary to resample $\vec{E}(t)$ at high resolution with equidistant time steps. The step width must be such that *both* $\vec{E}(t)$ and $e^{-2\pi i \nu t}$ do not vary too much for *all* frequencies of interest. (12) also allows a different number of sample points for the frequency and time axis which is advantageous for fast varying time signals giving a comparatively broad, smooth frequency spectrum.

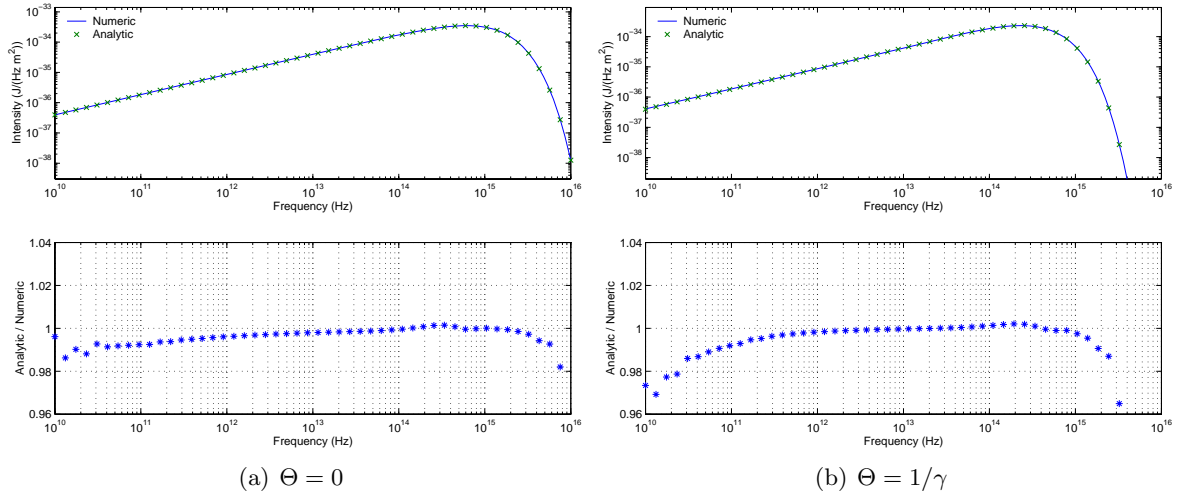


Figure 5 Comparison of the frequency dependence of the numerical algorithm results with (6). The lower plot shows the ratio of analytical and numerical values.

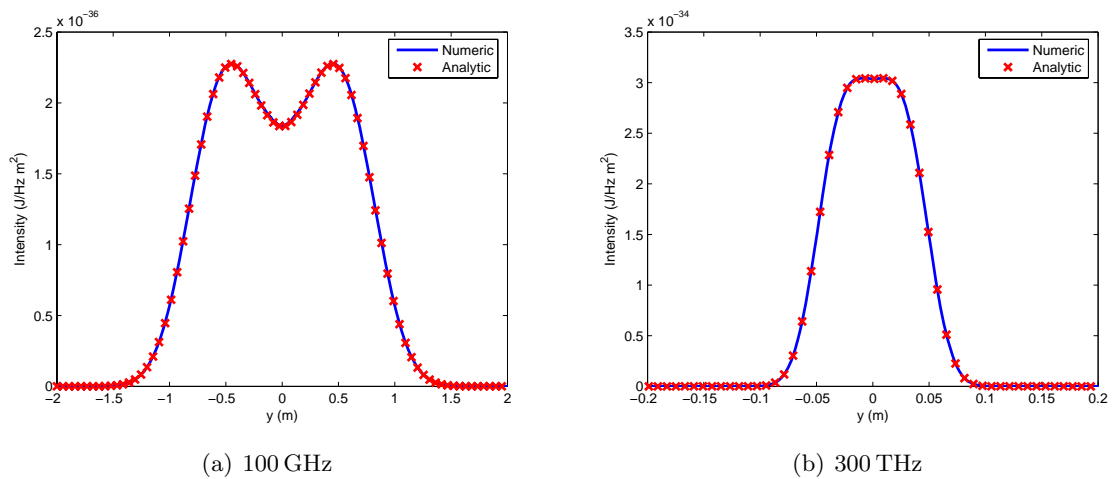


Figure 6 Comparison of the angular dependence of the numerical algorithm results with (6).

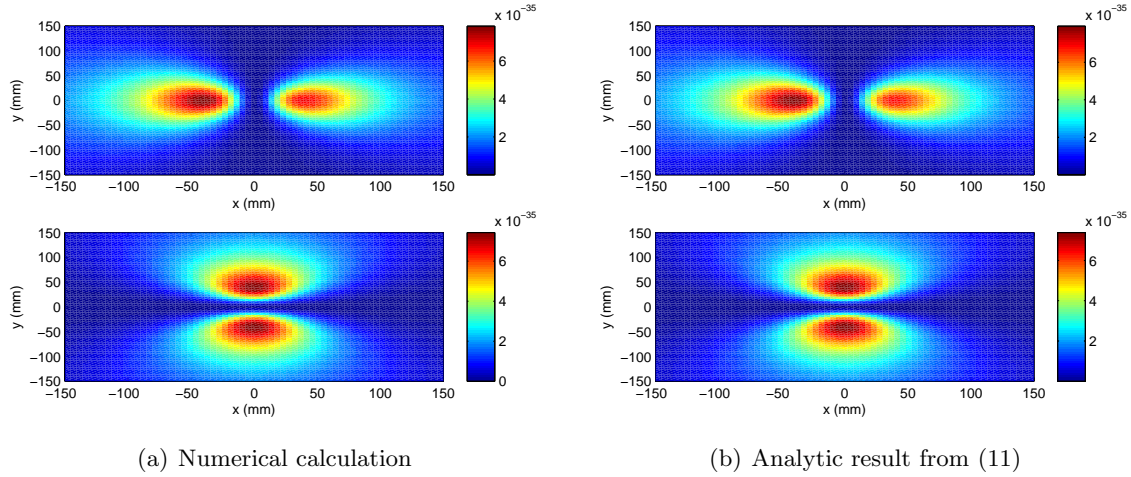


Figure 7 Comparison of the transverse intensity distribution for horizontal (top) and vertical (bottom) polarization for radiation dominated by the edge of the magnetic field.

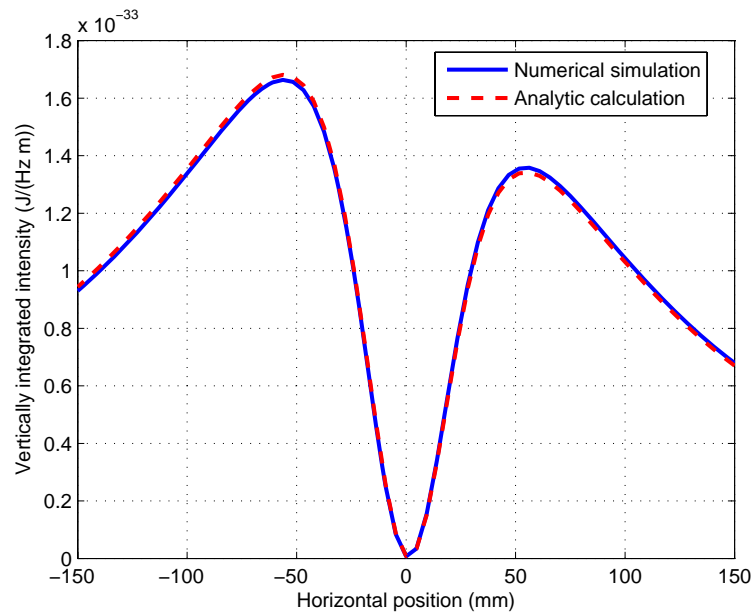


Figure 8 Vertical profiles of the horizontal polarization component shown in Fig. 7.

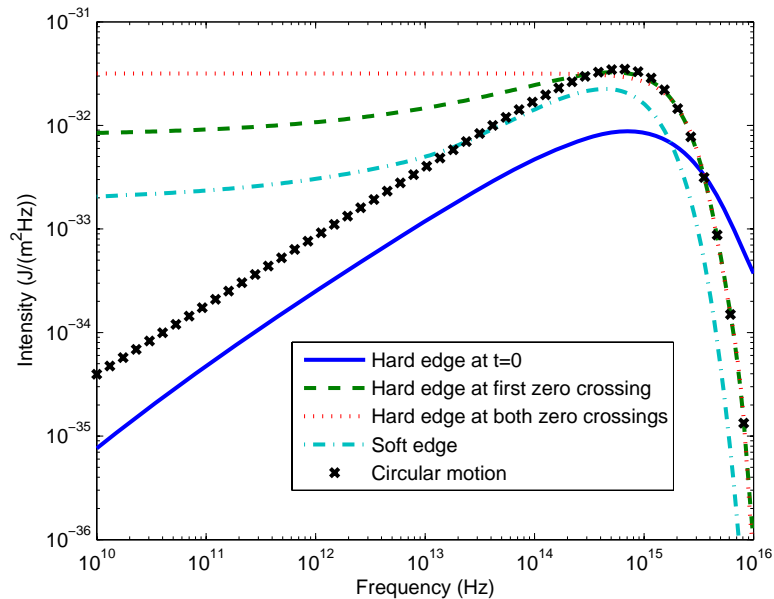


Figure 9 Radiation spectrum from a single dipole. For the hard edge cases, the observation point is tangentially to the trajectory at the edge, for the soft edge case slightly displaced in the bending direction. Circular motion is from (6).

3.3 Numerical results for a single magnet

Several peculiarities that occur in the spectra if only a magnet of finite length, especially with an edge, is considered can be seen in Fig. 9 in comparison to a spectrum resulting from circular motion in a constant magnetic field. The observation point is tangentially to the trajectory at 1 m distance from the entry edge. The hard edge, where the field jumps from 0 to 0.27 T instantaneously, is placed such that the acceleration term of the electric field in Fig. 2 is either cut at $t=0$ or at the first zero crossing. In the former case, the time integral is still zero⁶ and thus the spectrum drops towards long wavelength. The increased intensity at high frequencies is due to the sharp edge that is introduced in the time-domain electric field. Although the field already has a very fast rate of change even for circular motion in the vicinity of the spike, an ideal edge will of course imply even stronger Fourier components at high frequencies. In practice, best use of this effect requires placing the observation point within an angle better than $1/\gamma$ of the particle direction at the magnetic edge, and an edge that rises or falls significantly faster than this. For the soft edge case, the actual dependence of the field on the z coordinate as measured for a bunch compressor dipole was used.

The maximum low-frequency intensity can be achieved if a magnet that bends the electron by an angle of 2γ is used, as this will cut the electric field in time-domain at its zero crossings, maximizing the integral (see Sec. 2.2.1 and Fig. 2). The achievable intensity in forward direction can be calculated from the electric field (only the y component contributes):

$$E_y(\nu = 0) = \int_{-\infty}^{\infty} E_y(t) dt = 2 \int_0^{\frac{R}{\beta\gamma c}} E_y(t') \frac{1 + \alpha^2(t')\gamma^2}{2\gamma^2} dt'$$

⁶The time integral over the electric field pulse from circular motion is zero. Due to the symmetry of the field with respect to $t = 0$, this applies to either half of the field as well.

$$\begin{aligned}
&= \frac{2e}{4\pi\epsilon_0cL} \int_0^{1/\gamma} \frac{\beta^2 \sin^2 \alpha - \beta \cos \alpha + \beta^2 \cos^2 \alpha}{(1 - \beta \cos \alpha)^3} \frac{1 + \alpha^2 \gamma^2}{2\gamma^2} d\alpha \\
&= \frac{e}{4\pi\epsilon_0cL\gamma^2} \int_0^{1/\gamma} \frac{\beta - 1 + \frac{\alpha^2}{2}}{\left(1 - \beta + \frac{\beta\alpha^2}{2}\right)^3} (1 + \alpha^2 \gamma^2) d\alpha \\
&= \frac{e}{4\pi\epsilon_0cL\gamma^2} (2\gamma^2)^2 \underbrace{\int_0^{1/\gamma} \frac{\alpha^2 \gamma^2 - 1}{(\alpha^2 \gamma^2 + 1)^2} d\alpha}_{=-1/(2\gamma)}.
\end{aligned}$$

From (16), the energy per unit frequency per unit area becomes

$$\frac{d^2U}{d\nu dA}(\nu = 0) = \frac{2}{\mu_0 c} |E_y(\nu = 0)|^2 = \frac{e^2 \gamma^2}{2\pi^2 \epsilon_0 c L^2}.$$

Interestingly, this is independent of the magnetic field itself, though the length of the magnet has to be chosen to give a bend of 2γ . For the parameters taken in Fig. 9, the zero frequency intensity is $3.2 \cdot 10^{-32} \text{ J}/(\text{m}^2 \text{ Hz})$. The length of the radiation pulse in observer time is, from (8), twice the inverse of the critical angular frequency. For frequencies well below ω_c , the term νt in the Fourier transform (4) is very small, the exponential close to unity, and consequently the intensity is independent on the frequency in this region.

3.4 Two magnets

Radiation from the exit of the second-last and from the entrance of the last dipole magnet of the first FLASH bunch compressor will interfere for the geometry of the synchrotron radiation port, as seen in the particle trajectory in Fig. 10. The resulting electric field and spectrum are shown in Fig. 11.⁷ The field in time domain shows two spikes of opposite sign and different amplitude separated by $\Delta t = 5 \cdot 10^{-13} \text{ s}$. They result from the different bending direction and different distance to the detector of the two magnets. The spectrum has a similar envelope as in the case of circular motion, but overlaid with an oscillation with minima spaced in frequency by $1/\Delta t = 2 \cdot 10^{12} \text{ Hz}$. The integral over the field in time-domain is now nearly zero, so the spectrum drops towards lower frequencies as for circular motion. The amplitude of the oscillation depends on the relative size of the two spikes in the time-domain electric field.

The interference of the radiation contribution from both magnets is also apparent in the transverse intensity distribution, as seen in Fig. 12. The observation plane corresponds to the actual view port⁸, centered on the point indicated in Fig. 10. The top of the figure shows the distribution if only the radiation from the last magnet is considered, the bottom the fine structure that appears from the interference. It has to be kept in mind that these are single-electron spectra. The structures will be washed out if a bunch of finite size and divergence is considered.

3.5 Angular dependence of the spectrum

As was already seen in Fig. 5 for synchrotron radiation from circular motion, the spectrum depends on the observation angle. This is shown for four angles in Fig. 13 for the case of two

⁷The random-like structures seen in the spectrum at high frequencies are an artifact of the limited number of discrete frequencies for which the Fourier transform is calculated.

⁸The vacuum window is circular with 60 mm clear aperture, but the vertical dimension is determined by the vacuum chamber height.

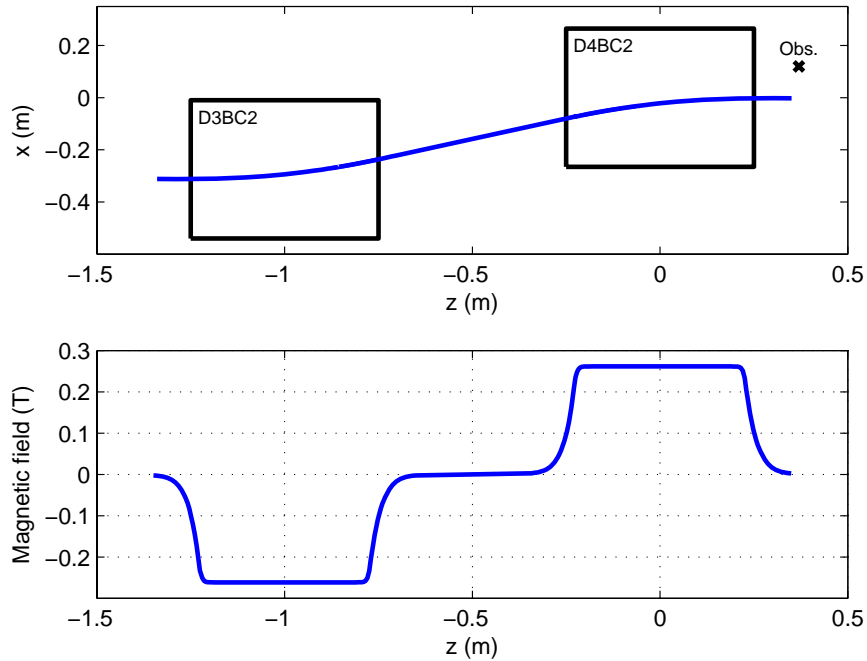


Figure 10 Particle trajectory through the last two magnets of the first bunch compressor of FLASH and the magnetic field. An observation point on the vacuum chamber view port is indicated.

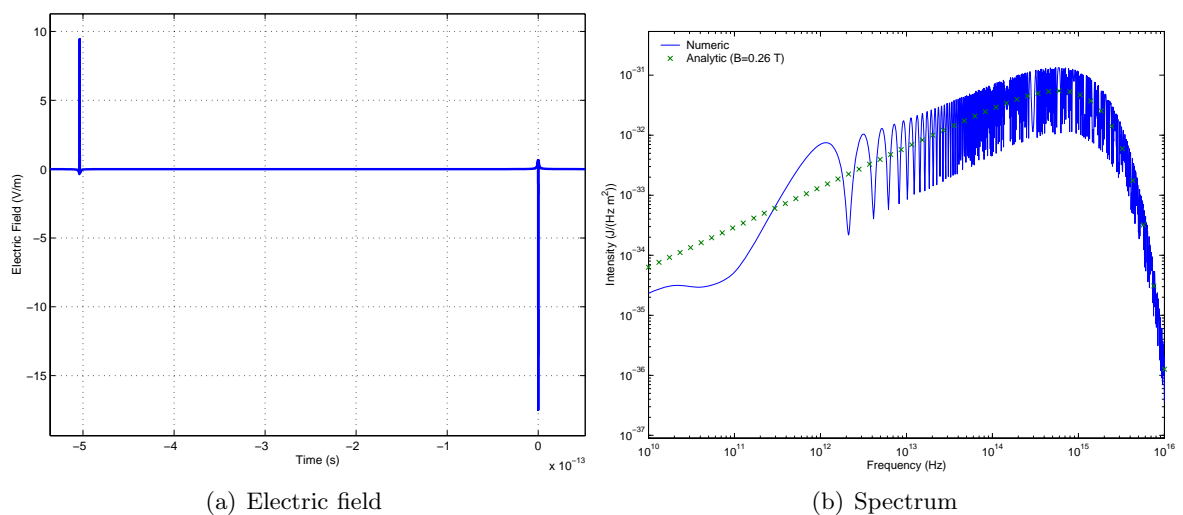


Figure 11 Radiation pulse and spectrum from two magnets. The observation point is along the axis defined by the straight part of the trajectory between the dipoles shown in Fig. 10.

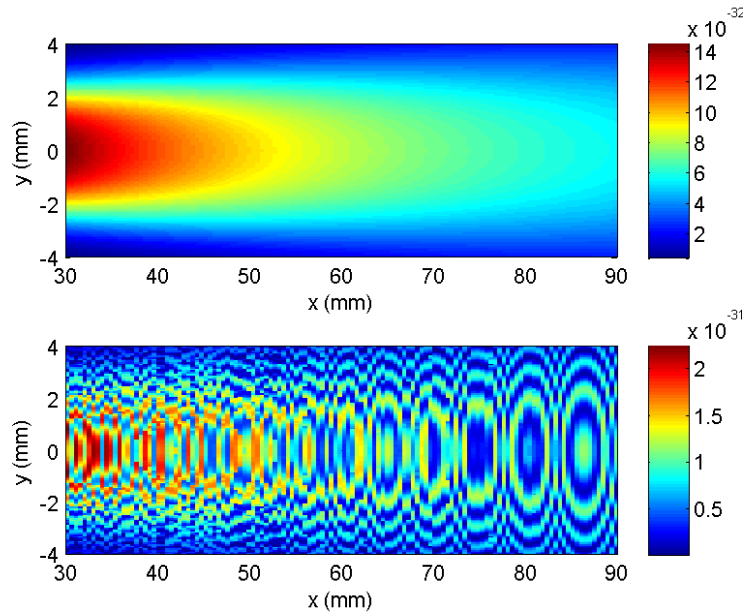


Figure 12 Interference effects on the transverse intensity distribution from two magnets (bottom) compared to the smooth distribution if only the second magnet is considered (top). The observation plane is centered on the point indicated in Fig. 10. The wavelength is $3\ \mu\text{m}$, horizontal polarisation. The colour scale is in units of $\text{J}/(\text{m}^2\text{Hz})$.

magnets as in the previous section.

The spectrum becomes softer at larger angles which is partly due to the angular dependence of the time compression factor (3). At an angle $1/\gamma$, this compression is only half as strong as on axis with zero angle.

3.6 Angular-integrated spectrum

The synchrotron radiation port of the first bunch compressor is $60\ \text{mm}$ wide and $8\ \text{mm}$ high. To estimate the average spectrum that a detector accepting all radiation that passes through this aperture will measure, the spectra at a number of points distributed over this area are calculated, multiplied by the area each one covers and then summed. The result is an energy spectrum in units of J/Hz . Because of symmetry, it suffices to calculate spectra above the plane of the particle trajectory.

The resulting averaged spectra are shown in Fig. 14 for a number of calculation grids ranging from a single point to 16×16 . An even higher resolution than a 16×16 point grid is necessary at the long wavelength end to achieve a stable result independent of this particular numerical parameter. The structures seen in Fig. 13 are washed out considerably due to the averaging.

If one half of the radiation port is covered, the spectrum changes as shown in Fig. 15. The spectrum is dominated by the half that is fully swept over by the synchrotron radiation beam. The spectrum through the other half is weaker and much softer. Tuning of this sort can be used to suppress the short wavelength components that don't carry any coherent information but would still saturate a frequency-integrating detector. However, as this comes at significant loss of intensity of also the desired wavelengths, wavelength filters will presumably be a better option for tailoring the spectrum.

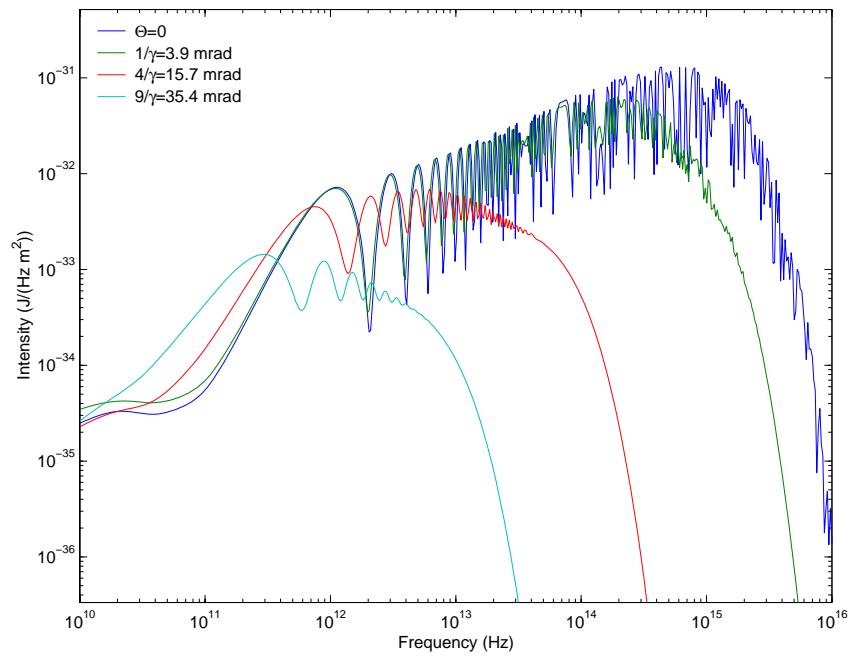


Figure 13 Dependency of the spectrum on the observation angle Θ

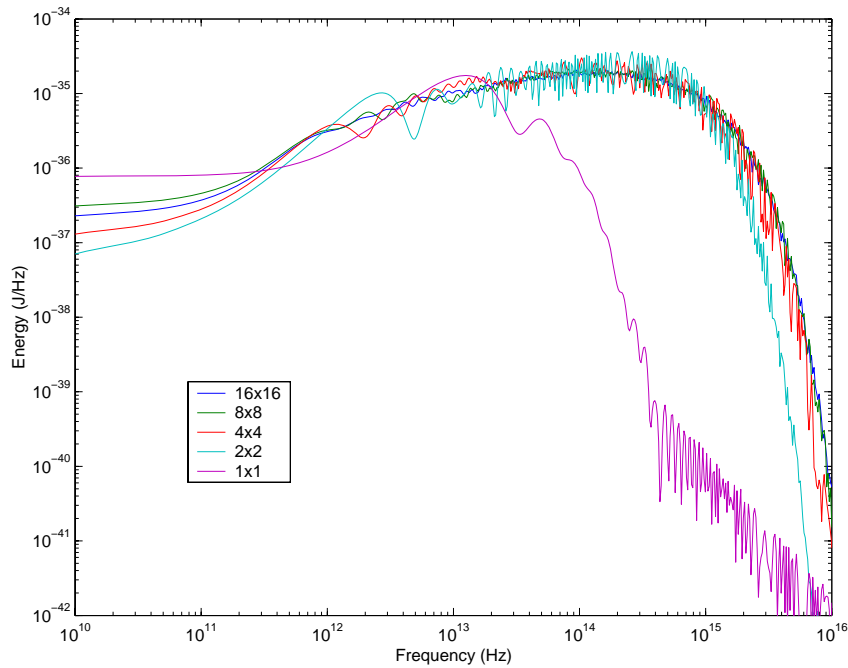


Figure 14 Dependency of the average spectrum on the calculation grid

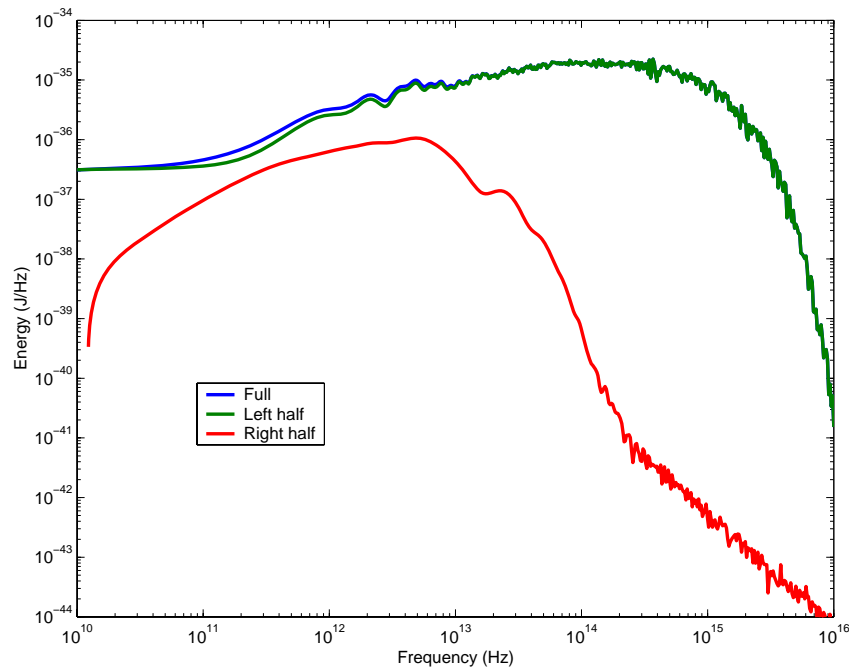


Figure 15 Average spectrum if only one half of the radiation port is open. 'Left half' refers to the half that is closer to the outgoing beam axis. Grid 8×8 .

3.7 Contribution from the velocity term

The calculations reported in the previous sections took into account only the acceleration term of the electric field in (1a), and used (16) to calculate the energy flow in frequency domain. It is shown here that the velocity term contributes very little even at comparatively small distances.

For the case of circular motion of an electron at 130 MeV in a field of 0.27 T and a distance to the detector of 1 m, both contributions to the electric field are shown in Fig. 2. The electric field from the velocity term at this distance is about two orders of magnitude smaller than the acceleration term. The contributions to the spectrum of both terms are shown separately in Fig. 16 for two smaller distances. The calculations makes use of the general expression (15). Only for the case of 15 mm does the velocity field contribute significantly, and predominantly so at low frequencies. Already at 15 cm distance its influence is negligible.

The sum of the individually computed spectral contributions of acceleration and velocity term is not equal to the result from a calculation taken the full expression of the electric field into account, as clearly expected since the intensity involves the square of the fields. In any case, the separation into acceleration and velocity term is artificial, and only useful to illustrate the relative significance. Only the full equation (1a) is a valid solution of the Maxwell equations.

3.8 Chamber cut-off

Wavelengths that would be emitted by an electron traversing a magnetic field in free space can be suppressed in the presence of metallic walls, for example from the vacuum chambers, as the fields need to fulfill additional boundary conditions. This shielding is for general boundary conditions hard to calculate, but a straightforward implementation is possible if the boundary is modeled as infinitely large, perfectly conducting plane-parallel plates. This is in fact a useful model for typical flat bunch compressor chambers.

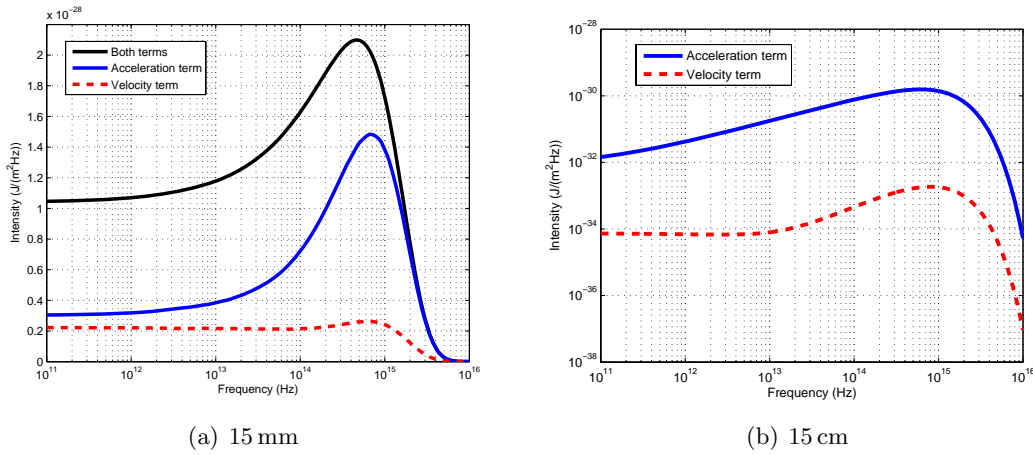


Figure 16 Comparison of spectral contribution of acceleration and velocity term for circular motion for two distances. For better illustration, one vertical scale is linear, one is logarithmic. The radius of curvature is 1.6 m. In (b), the result with both terms is indistinguishable on this scale from the acceleration term only.

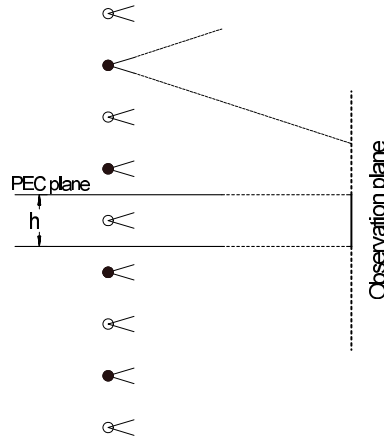


Figure 17 Infinitely large, perfectly conducting planes (PEC) can be replaced by mirror charges of alternating sign. Each charge emits synchrotron radiation into identical, finite cones, so only a limited number will interfere on an observation point between the plates.

In this case, the walls, separated by distance h , can be replaced by mirror charges of alternating sign, placed at distance h from each other as depicted in Fig. 17. The mirror charges are offset vertically from the actual charge, but otherwise are thought of as experiencing exactly the same magnetic field and thus the same acceleration. Each of these charges has a matching charge of opposite sign opposite to either of the two planes, so clearly the condition of vertical electric field on the boundaries is fulfilled.

The number of mirror charges that needs to be taken into account in practice is limited by the finite opening angle of the radiation cone and the limited region between the planes over which the field needs to be calculated. For an infinite number of mirror charges, the field distribution repeats periodically in the vertical, but according to the model the field is sensibly defined only between the plates.

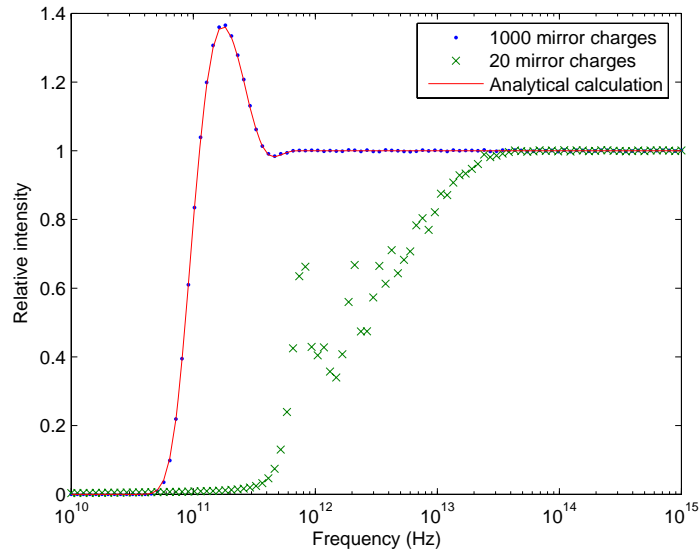


Figure 18 Analytical [Dohl98] and numerical calculation of the chamber cut-off for circular motion.

In [War90] a typical cut-off wavelength for electrons in circular motion with bending radius R was determined as $2h\sqrt{h/R}$. For the first bunch compressor, with $h=8$ mm, this cut-off is at 1.1 mm. For much shorter wavelengths the spectrum is unaffected, for much longer ones it is completely suppressed. Note, though, that again the condition of circular motion is in reality not fulfilled.

In [Dohl98], a cut-off function is calculated (also for circular motion) as reproduced in Fig. 18 for 10 m observation distance and the parameters of the first bunch compressor. The plot shows also a comparison with a numerical calculation. The necessary number of mirror charges can be estimated using the typical opening angle of synchrotron radiation in the far-infrared (10). On the observation plane at 10 m distance this gives a height of 2 m, and therefore the relevant number of mirror charges is a few times $2\text{ m}/8\text{ mm}=250$. This is supported by the comparison, which perfectly reproduces the analytical interference structure resulting from the mirror charges if 1000 such charges are considered, but fails for only 20.

This requires a lot of computation time, as the simple implementation of the numerical calculation tracks each mirror charge individually and then adds its electric field contribution in frequency domain at a particular observation point. The numerical simulation allows, however, to take into account a flat vacuum chamber for any magnetic field. This can result in very different shielding behaviour than for circular motion, as seen in Fig. 19. The plot shows the ratio of the average spectrum through the first bunch compressor view port (calculated with a high resolution of 128×128) with and without mirror charges, that is the shielding function analogous to Fig. 18. The shielding results in a concentration of energy close to the cut-off which is much more pronounced than for circular motion. There is also some significant difference if the interference from the third magnet is included in the calculation as well.

The calculation presented in Fig. 19 includes 50 mirror charges above and below the bending plane, although approximately 15 mirror charges are already enough to well reproduce the cut-off shape. This is very different than for circular motion, where many hundred mirror charges are necessary. This reflects the much stronger collimation of radiation that is predominately emitted from the edge of a magnetic field: for circular motion and the parameters of a bunch compressor

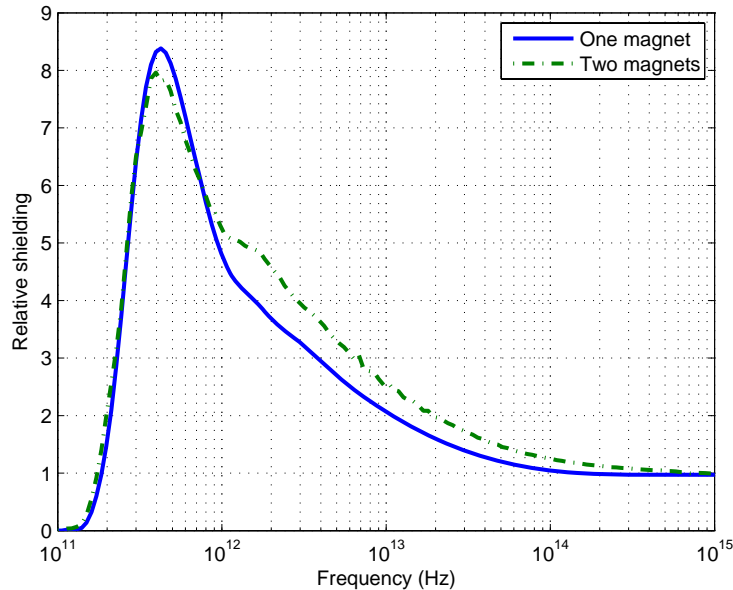


Figure 19 Shielding function for the radiation port of the first bunch compressor with and without consideration of interference from the third magnet. 50 mirror charges are taken into account.

magnet, the typical opening angle at 1 mm wavelength is, from (10), 67 mrad, whereas long-wavelength edge radiation has an angle of $1/\gamma$ or 4 mrad.

The most obvious effect of the inclusion of mirror charges on the transverse intensity distribution is that the horizontal polarization component vanishes on the conducting walls as seen in Fig. 20. This is clearly required by the boundary condition that is modelled with the mirror charges. At shorter wavelength, fine structures also appear on the intensity distribution. Only one magnet is considered here. Interference from a second magnet will add further structures.

An interesting point is that the cut-off can only be correctly reproduced in the numerical simulations if the velocity term of the electric field is included. Without it, a constant non-vanishing value of the spectrum appears at low frequencies. Despite this, it is sufficient to use (16) instead of (15) for calculation of the spectrum. This indicates that the velocity term contribution perpendicular to the unit vector \vec{n} is of importance and underlines that the velocity term can not always be neglected.

Further background information on shielding effects can be found in [Nod54, Bos02].

4 Results for FLASH

This section will briefly summarize numerical results that are relevant for the application of electron beam diagnostics with synchrotron radiation at FLASH. The average spectra for each case are useful to estimate the expected measurement signal in practice once it is known at one location.

4.1 Bunch compressors

The first bunch compressor operates at a beam energy of about 130 MeV. It consists of four magnets, arranged in an C-shape [Stu04], and has a view port of 60 mm width and 8 mm height

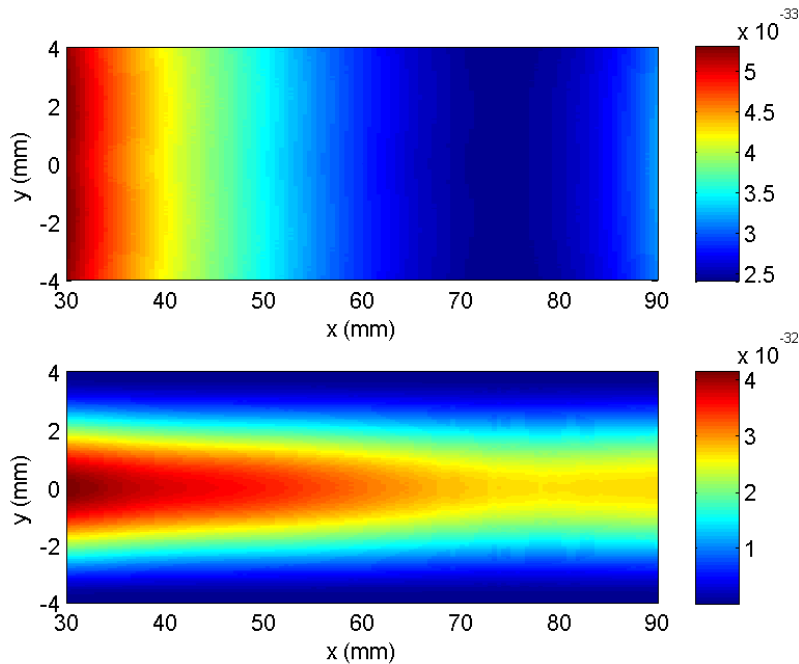


Figure 20 Effect of mirror charges on the transverse intensity distribution (bottom) compared to the case without mirror charges (top). The observation plane is centered on the point indicated in Fig. 10. The wavelength is $500\ \mu\text{m}$, horizontal polarisation. The colour scale is in units of $\text{J}/(\text{m}^2\text{Hz})$.

(determined by the vacuum chamber height) to couple out radiation from the last two magnets. The electron trajectory is shown in Fig. 10.

The second bunch compressor is in the form of an S-shaped chicane consisting of six magnets and is operated nominally at 380 MeV and with a deflection of 3.6° (radius of curvature 8 m). The individual magnets are similar to those of the first bunch compressor, the vacuum chamber has the same height. The view port is $26 \times 8\ \text{mm}^2$.

A comparison between the synchrotron radiation energy spectrum integrated over the respective view ports for the two bunch compressors is shown in Fig. 21. The total synchrotron radiation power, scaling after (9) as E^4/R^2 , is three times higher at the second bunch compressor, the solid angle of the view port is about 1/20 that of the first bunch compressor. The ratio of this is 6.6. The ratio of the total energy under the curves in the figure is about 4.

These spectra are approximations of the incoherent spectrum to be used for extracting the bunch form factor from measured spectra. Not yet taken into account here is the actual geometry of the vacuum chamber other than its finite height, which will further modify the spectrum (see [Pae08] for calculations in a more complete geometry), and, of course, any effects of the beam transport line and detection system.

The transverse intensity distribution at $50\ \mu\text{m}$ wavelength for both polarisations are shown in Fig. 22.

These calculations are done for the nominal trajectory through the bunch compressors. An analysis of a measurement of longitudinal structure should use calculations repeated for the actual, measured trajectory.

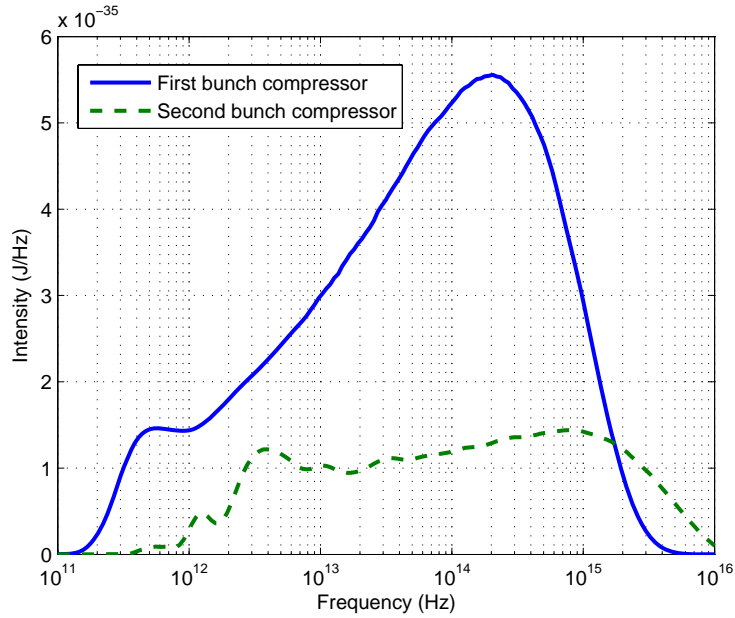


Figure 21 Single electron spectrum through the view ports of the first and second bunch compressors (130 MeV/18° and 380 MeV/3.6°). 50 mirror charges and interference from last two dipole magnets taken into account.

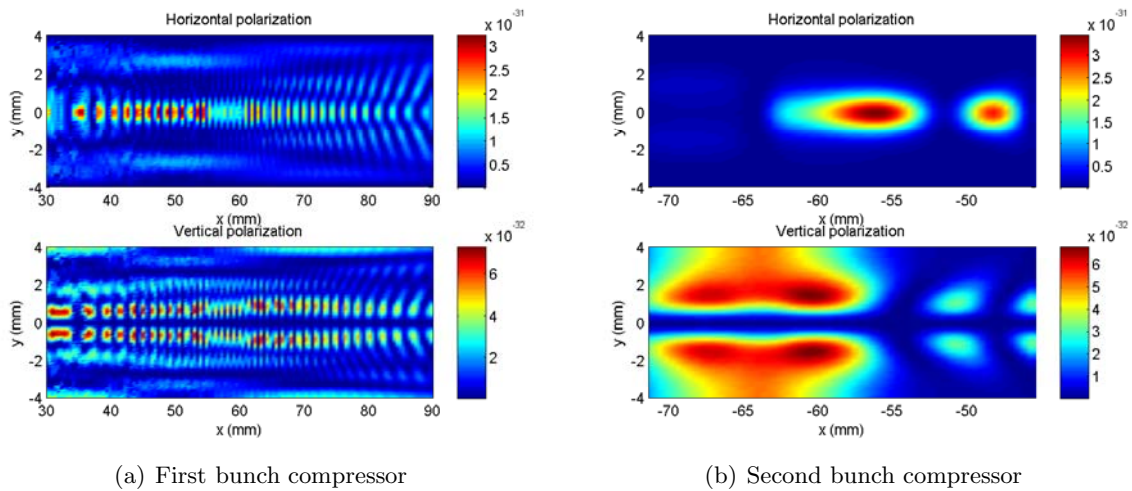


Figure 22 Transverse intensity distribution on the view ports of both bunch compressors at 50 μm . 50 mirror charges and interference from last two dipole magnets taken into account. The colour scale is in units of $\text{J}/(\text{m}^2\text{Hz})$.

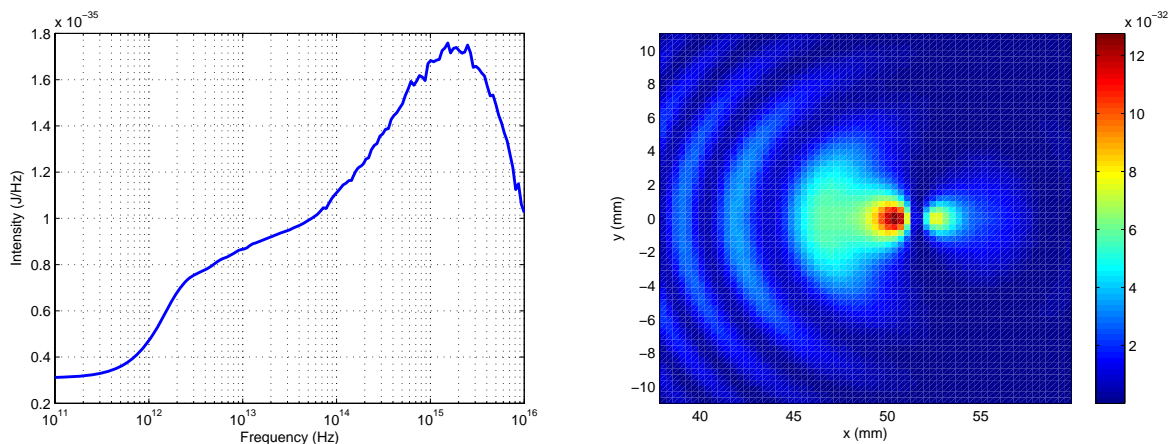


Figure 23 Single electron spectrum without shielding integrated over the view port of the second energy collimator dipole and transverse intensity distribution at 10 THz. Energy 511 MeV. The colour scale is in units of $\text{J}/(\text{m}^2\text{Hz})$.

4.2 Energy collimator

To remove off-energy electrons from the beam before passing the radiation-sensitive FEL undulators, an energy collimator is installed in FLASH. It consists of two dipole magnets, deflecting the beam by nominally 3.5° in opposite directions, and so offsetting the beam horizontally by 40 cm.

The second dipole has a small view port of 22 mm diameter. The spectrum, including interference effects from the first dipole, passing this port at 511 MeV electron energy is shown in Fig. 23, as well as the transverse intensity distribution at 10 THz. The interference is weak since the separation of the dipoles is 6.5 m. Mirror charges have not been considered, as the vacuum chamber has a height of 34 mm and suppression of the spectrum will only start at about 4 mm wavelength or 75 GHz frequency. The typical synchrotron radiation fan, starting about in the middle of the view port, becomes apparent at higher frequencies.

4.3 Infrared undulator

The FLASH electromagnetic infrared undulator, installed after the FEL undulators, uses the electron beam to generate pulses of radiation between $1 \mu\text{m}$ and $200 \mu\text{m}$ synchronized to the FEL pulses. As undulator radiation is the result of synchrotron radiation emission from a periodic magnetic structure, the single-electron emission spectrum of the undulator can be calculated using the numerical code presented here as well. However, the computation time becomes very long when using the general time-domain approach.⁹ The results presented in this subsection were therefore calculated using the paraxial approximation from [Gel05], decreasing the computation time by more than two orders of magnitude. Beforehand, it was verified that there is agreement with the general approach for several points.

As the undulator has only 9 periods, the harmonics in the spectrum are relatively wide with a bandwidth of about 10%, and pronounced oscillations occur between the peaks, as can be seen in the on-axis spectrum in Fig. 24 calculated for a K value of 30, an electron energy of 511 MeV, and a distance of 10 m behind the centre of the undulator. The high K value results in a wiggler

⁹The reason is that the formation length is the full undulator, 4.3 m. The procedure to adapt the size of the time steps and thus reduce computation time does not work efficiently in this case.

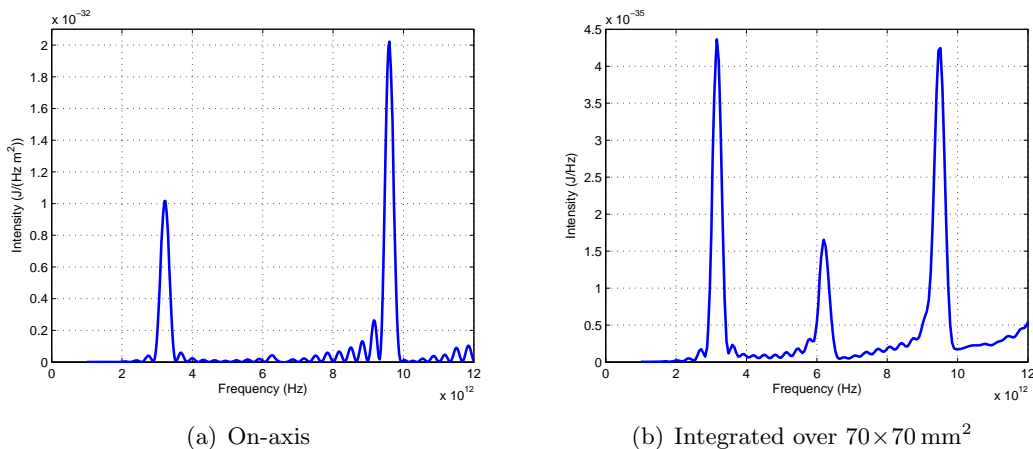


Figure 24 Infrared undulator spectra at $K=30$, 10 m behind the centre of the undulator.

spectrum with many harmonics, the third being visible. When integrating this over $70 \times 70 \text{ mm}^2$, corresponding approximately to the size of the beam line outcoupling mirror, also the second harmonic appears, and the oscillations start to merge into a rising, continuous spectrum. At higher frequencies, the spectrum will approach that of synchrotron radiation from circular motion.

5 Conclusions

This report gave a concise overview of the basic procedures to calculate synchrotron radiation spectra and listed some major analytical results for special cases. A simple numerical algorithm to calculate spectra for general magnetic fields was presented, together with a verification of some results against analytical calculations. Finally, specific results applicable to beam diagnostics with synchrotron radiation at FLASH were presented.

It should be stressed that the *raison d'être* of such a code lies mainly in the full control of its internal functioning. Compared to other codes, like for example SRW, the code is slow, but, as it employs no approximations to speed up the calculations, it should give correct results for arbitrary magnetic fields once the independence from numerical integration parameters has been checked. It can thus be used as a more advanced benchmarking for faster, optimized codes than analytical calculations alone.

Acknowledgments

Helpful discussions with H. Delsim-Hashemi and A. Willner contributed to this paper. Their meticulous reading of the manuscript eliminated numerous mistakes.

A Derivation of the frequency spectrum

The explicit procedure to deduce the energy spectrum in frequency domain from the time-dependent electric field $\vec{E}(t)$ emitted by a single accelerated charge via Fourier transformation is

shown here. To this end, first the straightforward time-domain expression for the Poynting vector will be deduced, then the corresponding frequency-domain expression and its interpretation. Finally, the energy flow for synchrotron radiation is calculated. All calculations are done for free space, so the relative dielectric constant and permeability are taken as unity.

A.1 Poynting vector in time domain

The Maxwell equations in time domain are

$$\begin{aligned}\vec{\nabla} \cdot \vec{E}(t) &= \frac{1}{\epsilon_0} \rho(t), & \vec{\nabla} \times \vec{E}(t) &= -\frac{\partial \vec{B}(t)}{\partial t}, \\ \vec{\nabla} \cdot \vec{B}(t) &= 0, & \vec{\nabla} \times \vec{B}(t) &= \mu_0 \vec{j}(t) + \epsilon_0 \mu_0 \frac{\partial \vec{E}(t)}{\partial t},\end{aligned}\tag{13}$$

where $\rho(t)$ is the charge density and $\vec{j}(t)$ the current density. The mechanical work per unit time and volume done by the field on the charge density is given by $\vec{E}(t) \cdot \vec{j}(t)$, and can be expressed as

$$\begin{aligned}\vec{E}(t) \cdot \vec{j}(t) &= \frac{1}{\mu_0} \vec{E}(t) \cdot \left(\vec{\nabla} \times \vec{B}(t) - \epsilon_0 \mu_0 \frac{\partial \vec{E}(t)}{\partial t} \right) \\ &= \frac{1}{\mu_0} \left[\vec{B}(t) \cdot \left(\vec{\nabla} \times \vec{E}(t) \right) - \vec{\nabla} \cdot \left(\vec{E}(t) \times \vec{B}(t) \right) - \epsilon_0 \mu_0 \vec{E}(t) \cdot \frac{\partial \vec{E}(t)}{\partial t} \right] \\ &= \frac{1}{\mu_0} \left[-\vec{B}(t) \cdot \frac{\partial \vec{B}(t)}{\partial t} - \vec{\nabla} \cdot \left(\vec{E}(t) \times \vec{B}(t) \right) - \epsilon_0 \mu_0 \vec{E}(t) \cdot \frac{\partial \vec{E}(t)}{\partial t} \right] \\ &= -\frac{\partial}{\partial t} \left(\frac{\vec{B}^2(t)}{2\mu_0} + \frac{\epsilon_0 \vec{E}^2(t)}{2} \right) - \frac{1}{\mu_0} \vec{\nabla} \cdot \left(\vec{E}(t) \times \vec{B}(t) \right).\end{aligned}$$

Integrating this over a volume V bounded by area A yields, through application of the divergence theorem (assuming that there are no singularities within the volume), the Poynting theorem

$$\int_V \vec{E}(t) \cdot \vec{j}(t) dV = -\frac{\partial}{\partial t} \int_V \underbrace{\left(\frac{1}{2\mu_0} \vec{B}^2(t) + \frac{\epsilon_0}{2} \vec{E}^2(t) \right) dV}_{u(t)} - \oint_A \underbrace{\left(\frac{1}{\mu_0} \vec{E}(t) \times \vec{B}(t) \right) \cdot d\vec{A}}_{\vec{S}(t)}.$$

The surface element $d\vec{A}$ is normal to the surface. The left-hand side represents the total mechanical work per unit time done on the charges within V , allowing to identify the energy density $u(t)$ and the power flow $\vec{S}(t)$, called the Poynting vector.

A.2 Poynting vector in frequency domain

Defining the Fourier transforms $\vec{E}(\nu)$, $\vec{B}(\nu)$, $\rho(\nu)$ and $\vec{j}(\nu)$ according to (4), and inserting into (13) yields the Maxwell equations in frequency domain. As an example,

$$\vec{\nabla} \times \vec{B}(t) = \vec{\nabla} \times \int_{-\infty}^{\infty} \vec{B}(\nu) e^{2\pi i \nu t} d\nu = \mu_0 \int_{-\infty}^{\infty} \vec{j}(\nu) e^{2\pi i \nu t} d\nu + \epsilon_0 \mu_0 \frac{\partial}{\partial t} \int_{-\infty}^{\infty} \vec{E}(\nu) e^{2\pi i \nu t} d\nu.$$

Interchanging integration and differentiation yields

$$\int_{-\infty}^{\infty} \left(\vec{\nabla} \times \vec{B}(\nu) - \mu_0 \vec{j}(\nu) - 2\pi i \epsilon_0 \mu_0 \nu \vec{E}(\nu) \right) e^{2\pi i \nu t} d\nu = 0,$$

which has to hold for all t and therefore requires

$$\vec{\nabla} \times \vec{B}(\nu) = \mu_0 \vec{j}(\nu) + 2\pi i \epsilon_0 \mu_0 \nu \vec{E}(\nu).$$

Similar for the other equations, yielding the set of Maxwell equations in frequency domain:

$$\begin{aligned} \vec{\nabla} \cdot \vec{E}(\nu) &= \frac{1}{\epsilon_0} \rho(\nu), & \vec{\nabla} \times \vec{E}(\nu) &= -2\pi i \nu \vec{B}(\nu), \\ \vec{\nabla} \cdot \vec{B}(\nu) &= 0, & \vec{\nabla} \times \vec{B}(\nu) &= \mu_0 \vec{j}(\nu) + 2\pi i \epsilon_0 \mu_0 \nu \vec{E}(\nu). \end{aligned}$$

Multiplying the rotation equation involving $\vec{E}(\nu)$ with $-\vec{B}^*(\nu)/\mu_0$, taking the complex conjugate rotation equation involving $\vec{B}(\nu)$ and multiplying it with $\vec{E}(\nu)$, and then adding both results in

$$\begin{aligned} \vec{E}(\nu) \cdot (\vec{\nabla} \times \vec{B}^*(\nu)) - \vec{B}^*(\nu) \cdot (\vec{\nabla} \times \vec{E}(\nu)) &= -\vec{\nabla} \cdot (\vec{E}(\nu) \times \vec{B}^*(\nu)) \\ &= 2\pi i \nu \left(|\vec{B}(\nu)|^2 - \epsilon_0 \mu_0 |\vec{E}(\nu)|^2 \right) + \mu_0 \vec{E}(\nu) \cdot \vec{j}^*(\nu). \end{aligned}$$

Again through application of the divergence theorem, an integration over a volume V bounded by area A yields

$$\int_V \vec{E}(\nu) \cdot \vec{j}^*(\nu) dV = 2\pi i \nu \int_V \epsilon_0 |\vec{E}(\nu)|^2 - \frac{1}{\mu_0} |\vec{B}(\nu)|^2 dV - \oint_A \underbrace{\left(\frac{1}{\mu_0} \vec{E}(\nu) \times \vec{B}^*(\nu) \right)}_{\vec{S}(\nu)} \cdot d\vec{A},$$

defining the frequency-domain Poynting vector $\vec{S}(\nu)$.

$\vec{S}(\nu)$ is a complex quantity, its significance with respect to energy transport is therefore not immediately obvious. To clarify the connection, consider that the time-integrated time-domain Poynting vector must yield the same result as a suitably chosen quantity when frequency integrated. As frequencies should be non-negative, the relation can be deduced as follows:

$$\begin{aligned} \int_{-\infty}^{\infty} \vec{S}(t) dt &= \frac{1}{\mu_0} \int_{-\infty}^{\infty} \vec{E}(t) \times \vec{B}(t) dt = \frac{1}{\mu_0} \int_{-\infty}^{\infty} \int_{-\infty}^{\infty} \vec{E}(\nu) e^{2\pi i \nu t} d\nu \times \int_{-\infty}^{\infty} \vec{B}(\nu') e^{2\pi i \nu' t} d\nu' dt \\ &= \frac{1}{\mu_0} \int_{-\infty}^{\infty} \int_{-\infty}^{\infty} \vec{E}(\nu) \times \vec{B}(\nu') \int_{-\infty}^{\infty} e^{2\pi i (\nu + \nu') t} dt d\nu d\nu' \\ &= \frac{1}{\mu_0} \int_{-\infty}^{\infty} \vec{E}(\nu) \times \vec{B}(\nu') \delta(\nu + \nu') d\nu d\nu' \\ &= \frac{1}{\mu_0} \int_{-\infty}^0 \vec{E}(\nu) \times \vec{B}(-\nu) d\nu + \frac{1}{\mu_0} \int_0^{\infty} \vec{E}(\nu) \times \vec{B}(-\nu) d\nu \\ &= \frac{1}{\mu_0} \int_0^{\infty} \left(\vec{E}(-\nu) \times \vec{B}(\nu) + \vec{E}(\nu) \times \vec{B}(-\nu) \right) d\nu \\ &= \frac{1}{\mu_0} \int_0^{\infty} \left(\vec{E}^*(\nu) \times \vec{B}(\nu) + \vec{E}(\nu) \times \vec{B}^*(\nu) \right) d\nu \quad \text{by using (4)} \end{aligned}$$

$$= \frac{2}{\mu_0} \int_0^{\infty} \Re \left\{ \vec{E}(\nu) \times \vec{B}^*(\nu) \right\} d\nu = 2 \int_0^{\infty} \Re \left\{ \vec{S}(\nu) \right\} d\nu.$$

Twice the real part of the frequency-domain Poynting vector gives therefore the desired energy per unit area per unit frequency.

To illuminate the relation from a different side, consider a complex oscillating electric field $\tilde{E}(t, \nu) = \vec{E}(\nu) e^{2\pi i \nu t}$, $\vec{E}(\nu) = \tilde{E}_r(\nu) + i\tilde{E}_i(\nu)$, $\tilde{E}_r(\nu)$ and $\tilde{E}_i(\nu)$ real, and similarly for the magnetic field.¹⁰ A real time domain field is then, for example,

$$\vec{E}(t, \nu) = \Re \left\{ \tilde{E}(t, \nu) \right\} = \Re \left\{ (\tilde{E}_r + i\tilde{E}_i)(\cos 2\pi\nu t + i \sin 2\pi\nu t) \right\} = \tilde{E}_r(\nu) \cos 2\pi\nu t - \tilde{E}_i(\nu) \sin 2\pi\nu t.$$

The time-averaged time-domain Poynting vector for the electric and magnetic field thus defined is

$$\overline{\vec{S}(t)} = \frac{1}{\mu_0} \overline{\vec{E}(t, \nu) \times \vec{B}(t, \nu)} = \frac{1}{2\mu_0} \left(\tilde{E}_r(\nu) \times \tilde{B}_r(\nu) + \tilde{E}_i(\nu) \times \tilde{B}_i(\nu) \right).$$

The real part of the frequency-domain Poynting vector is

$$\Re \left\{ \vec{S}(\nu) \right\} = \frac{1}{\mu_0} \Re \left\{ (\tilde{E}_r(\nu) + i\tilde{E}_i(\nu)) \times (\tilde{B}_r(\nu) + i\tilde{B}_i(\nu)) \right\} = \frac{1}{2} \overline{\vec{S}(t)}.$$

The real part of the complex frequency-domain Poynting vector is equal to half of the time-averaged time-domain Poynting vector.

A.3 Energy transport for synchrotron radiation

The energy that crosses an area dA per unit time, i.e. the power density $d^2U/(dt dA)$ at a certain position is given by the absolute magnitude of the time-domain Poynting vector $\vec{S}(t)$ deduced in Appendix A.1 above. Using the expression (1b) for the magnetic field from an accelerated charge, the Poynting vector becomes

$$\vec{S}(t) = \frac{1}{\mu_0 c} \vec{E}(t) \times \left(\vec{n}(t') \times \vec{E}(t) \right) = \epsilon_0 c \left(\vec{E}^2(t) \vec{n}(t') - \left(\vec{E}(t) \cdot \vec{n}(t') \right) \vec{E}(t) \right),$$

where the retarded time $t' = t - R(t')/c$ (see Sect. 2). Note that this fully general expression assures that a stationary charge does not radiate, as then $\vec{E}(t)$ and $\vec{n}(t')$ are constant and parallel, and the second term then cancels the first. Due to the retardation, they are still parallel for a charge in uniform motion, assuring also in this case that no energy is radiated.

If only the acceleration term of (1a) is considered (large distance from the source region), $\vec{E}(t)$ and $\vec{n}(t')$ are perpendicular, thus in this case

$$\frac{d^2U}{dt dA} = \left| \vec{S}(t) \right| = \epsilon_0 c \vec{E}^2(t). \quad (14)$$

The units of this quantity are $\text{W}/\text{m}^2 = \text{J}/(\text{s}\text{m}^2)$. The direction of power flow, given by the direction of $\vec{S}(t)$, is in general not along $\vec{n}(t)$ except under this large distance condition.

The related quantity in frequency domain, the energy density spectrum $dU/d\nu$ at a given position is, following the above calculations,

$$\boxed{\frac{d^2U}{d\nu dA} = 2 \left| \Re \left\{ \vec{S}(\nu) \right\} \right| = 2 \left| \Re \left\{ \frac{1}{\mu_0} \vec{E}(\nu) \times \vec{B}^*(\nu) \right\} \right|}. \quad (15)$$

¹⁰These can essentially be thought of as individual components of the inverse Fourier transform of (4).

If the unit vector \vec{n} is assumed to be constant, thus $\vec{B}(t) = \vec{n} \times \vec{E}(t)/c$, the Fourier transform of the magnetic field is simply $\vec{B}(\nu) = \vec{n} \times \vec{E}(\nu)/c$. If also only the acceleration term of the electric field is considered¹¹, it follows that

$$\begin{aligned} \frac{d^2U}{d\nu dA} &= \frac{2}{\mu_0} \left| \Re \left\{ \vec{E}(\nu) \times \frac{1}{c} \left(\vec{n} \times \vec{E}^*(\nu) \right) \right\} \right| \\ &= \frac{2}{\mu_0 c} \left| \Re \left\{ \vec{n} \left(\vec{E}(\nu) \cdot \vec{E}^*(\nu) \right) - \vec{E}^*(\nu) \left(\vec{E}(\nu) \cdot \vec{n} \right) \right\} \right| = \frac{2}{\mu_0 c} \left| \vec{E}(\nu) \right|^2. \end{aligned} \quad (16)$$

The units are J/(Hz m²).

B Linear interpolation for numerical Fourier transformation

The discrete Fourier transform is given by (12) to zeroth order, i.e. $\vec{E}(t)$ is assumed to be constant within a time step. Using more adjacent points, a better interpolation can be made. The first order (linear interpolation) $\vec{E}_1(\nu_j)$ is shown here.

$$\begin{aligned} \vec{E}_1(\nu_j) &= \sum_i \int_{t_i}^{t_{i+1}} \left(\vec{E}(t_i) + \frac{\vec{E}(t_{i+1}) - \vec{E}(t_i)}{t_{i+1} - t_i} (t - t_i) \right) e^{-2\pi i \nu_j t} dt \\ &= \vec{E}_0(\nu_j) + \sum_i \frac{\vec{E}(t_{i+1}) - \vec{E}(t_i)}{t_{i+1} - t_i} \int_0^{t_{i+1} - t_i} x e^{-2\pi i \nu_j (x + t_i)} dx \quad (x = t - t_i) \\ &= \vec{E}_0(\nu_j) + \sum_i \frac{\vec{E}(t_{i+1}) - \vec{E}(t_i)}{t_{i+1} - t_i} e^{-2\pi i \nu_j t_i} \int_0^{t_{i+1} - t_i} x e^{-2\pi i \nu_j x} dx \\ &= \vec{E}_0(\nu_j) + \sum_i \frac{\vec{E}(t_{i+1}) - \vec{E}(t_i)}{t_{i+1} - t_i} e^{-2\pi i \nu_j t_i} \left[\frac{2\pi i \nu_j x + 1}{(2\pi \nu_j)^2} e^{-2\pi i \nu_j x} \right]_0^{t_{i+1} - t_i} \\ &= \vec{E}_0(\nu_j) + \sum_i \frac{\vec{E}(t_{i+1}) - \vec{E}(t_i)}{(2\pi \nu_j)^2 (t_{i+1} - t_i)} \left(e^{-2\pi i \nu_j t_{i+1}} (2\pi i \nu_j (t_{i+1} - t_i) + 1) - e^{-2\pi i \nu_j t_i} \right) \end{aligned} \quad (17)$$

It may however be computationally more economic to use a smaller step size and $\vec{E}_0(\nu)$ instead of this relatively complex expression for $\vec{E}_1(\nu)$

C Basic relations for an electron in a magnetic field

The circular trajectory of radius R of an electron in an homogeneous magnetic field B can be described by

$$x(t) = R \sin(2\pi \nu t), \quad y(t) = R(1 - \cos(2\pi \nu t)) \quad \implies \quad y(x) = R \left(1 - \cos \left(\arcsin \frac{x}{R} \right) \right)$$

where the electron passes at $t = 0$ through the coordinate origin and $\nu = c/(2\pi R)$. The deflection angle is

$$\tan \alpha(x) = \frac{dy}{dx} = \left(\left(\frac{R}{x} \right)^2 - 1 \right)^{-1/2}.$$

¹¹For \vec{n} time independent, (1a) and (4) result in $\vec{E}(\nu)$ being orthogonal to \vec{n} if the velocity term is neglected.

For an electron energy E , the radius of curvature for relativistic energies ($\gamma \gg 1$) is

$$R = \frac{E}{ecB} = \frac{mc\gamma}{eB}.$$

For a magnet with effective length l and a given angular deflection α

$$R = l\sqrt{\frac{1}{\tan^2\alpha} + 1} \quad (\alpha < 90^\circ).$$

The required magnetic field is

$$B = \frac{E}{ecl} \left(\frac{1}{\tan^2\alpha} + 1 \right)^{-1/2}.$$

As examples, take the first bunch compressor at FLASH: $E=130$ MeV, $l=50$ cm, $\alpha=18^\circ$ which results in $B=0.27$ T, $R=1.6$ m. For the second bunch compressor $E=380$ MeV, $l=50$ cm, $\alpha=3.6^\circ$ giving $B=0.16$ T, $R=8.0$ m.

The instantaneous acceleration $\dot{\vec{\beta}}(t) = \dot{\vec{v}}(t)/c$ of an electron by a magnetic field $B(t)$ is given through the Lorentz force as

$$\dot{\vec{\beta}}(t) = \frac{e}{m\gamma} \vec{\beta}(t) \times \vec{B}(t). \quad (18)$$

D Listing of the Matlab code

For reference, the essential parts of the SynchroSim Matlab code are listed here. It makes extensive use of matrix manipulations to take advantage of their fast computation. The full version of the code has several cases of interest for FLASH implemented. As this requires an external magnetic field definition file, these are not reproduced here. The code is available from the author.

```
% Coordinate system as for FLASH, vectors are x y z. Particle trajectory is assumed
% flat (confined to x/z plane). All calculations are done in SI units.

clear; close all;
c0 = 2.99792458e8; m0 = 9.109389e-31;
e0 = -1.602177e-19; epsilon0 = 8.854187e-12;

CalcMode = 0; % 0 time-domain with acc. term, 1 full time-domain, 2 parax. approximation
SimulationCase = 0;
Frequency = logspace(10,16,200);

NumMirror = 50; % Number of mirror charges above orbit plane
Nx = 64; Ny = 64; % Point grid for calculation

deltat = 3.33e-12; % Set according to scale of magnetic field changes
MaxSteps = 200000; % Maximum number of steps for tracking (to avoid infinite loops)
MaxFieldChange = 1e-4; % Maximum change of electric field magnitude in V/m per step
MaxDivider = 64; % Maximum reduction factor of step size if field change too fast

% =====
% End user data section
% =====

load MagFieldDef.mat;
switch SimulationCase
case 0 % Circular motion with the viewport midpoint tangent to the arc at z=0
WidthX = 0.06; WidthY = 0.06; % Width and height of viewport
MidPoint = [0 0 1]; ViewportAngle = 0; % Centre position and rotation of viewport
B=0.27; gamma = 254.4; % 130 MeV
InitialAngle = pi/3; % Initial angle and position of particle trajectory
InitialPosition = -m0*c0/e0*gamma/B*[-(1-cos(InitialAngle)) 0 -sin(InitialAngle)];
MagZPos = [InitialPosition(3) -InitialPosition(3)]; MagField = [B B];
otherwise
disp 'Unknow simulation case, terminating...';
return;
end
```

```

PosX = WidthX*linspace(-1/2,1/2,Nx) * (Nx~=1); % Positions where to calculate electric field
PosY = WidthY*linspace(-1/2,1/2,Ny) * (Ny~=1); % If only one point requested, use midpoint

DetectorPos = zeros(Nx*Ny,3);
ElectricField = zeros(MaxSteps-1,3); MagneticField = zeros(MaxSteps-1,3);
UnitVector = zeros(MaxSteps-1,3); FieldMagnitude = zeros(1,MaxSteps-1);
DetectorTime = zeros(1,MaxSteps-1); Trajectory = zeros(MaxSteps-1,2);
FourierX = zeros(Nx*Ny,length(Frequency)); FourierY = FourierX; FourierZ = FourierX;
FourierMagX = FourierX; FourierMagY = FourierX; FourierMagZ = FourierX;
IntensityAcc = zeros(Nx*Ny,length(Frequency)); TotalEnergy = zeros(Nx*Ny,1);

MFileContents = textread([filename('fullpath') '.m'],'s','delimiter','\n','whitespace',''); % Store contents for reference

%
% ++++++++ Main Program ++++++++
%
beta = sqrt(1-(gamma*gamma));
tic;
for k = 1:Nx*Ny % Loop over detector positions
    DetectorPos(k,:) = MidPoint + [cos(ViewportAngle)*PosX(floor((k-1)/Ny)+1) PosY(mod(k-1,Ny)+1) -sin(ViewportAngle)*PosX(floor((k-1)/Ny)+1)];
% Distribution of intensity is symmetrical about vertical axis, y component of electric field changes sign
if DetectorPos(k,2)>0 && MidPoint(2)==0
    FourierX(k,:) = FourierX(k-(2*find(PosY==DetectorPos(k,2))-Ny-1),:);
    FourierY(k,:) = -FourierY(k-(2*find(PosY==DetectorPos(k,2))-Ny-1),:);
    FourierZ(k,:) = FourierZ(k-(2*find(PosY==DetectorPos(k,2))-Ny-1),:);
    IntensityAcc(k,:) = IntensityAcc(k-(2*find(PosY==DetectorPos(k,2))-Ny-1),:);
    TotalEnergy(k) = TotalEnergy(k-(2*find(PosY==DetectorPos(k,2))-Ny-1));
    fprintf('Skipped position %d for symmetry...\n',k);
    continue;
end

for m = -NumMirror:NumMirror % Loop over mirror charges

Step=1; Divider=1; ParticleTime=0; LastDisplayTime=toc; IntEnergy=0;
ParticlePosition = InitialPosition+m*[0 WidthY 0]; Angle = InitialAngle;

while (ParticlePosition(3)<=max(MagZPos) && (Step<MaxSteps || CalcMode==2))

% Field calculation
UnitVecDetector = DetectorPos(k,:)-ParticlePosition;
Distance = sqrt(dot(UnitVecDetector,UnitVecDetector));
B = interp1(MagZPos, MagField, ParticlePosition(3), 'linear', 0);
if CalcMode==2 % Time-domain calculation
    betaDotVec = e0*B*beta/(gamma*m0)*[cos(Angle) 0 -sin(Angle)];
    UnitVecDetector = UnitVecDetector/Distance;
    betaVec = beta*[sin(Angle) 0 cos(Angle)];
    if CalcMode==0 % Only acceleration term
        ElectricField(Step,:) = (-1)^m*e0/(4*pi*epsilon0*(1-dot(betaVec,UnitVecDetector))^3*Distance)* ...
        (cross(UnitVecDetector,cross(UnitVecDetector-betaVec,betaDotVec))/c0);
    else % Velocity and acceleration term, and then also magnetic field
        ElectricField(Step,:) = (-1)^m*e0/(4*pi*epsilon0*(1-dot(betaVec,UnitVecDetector))^3*Distance)* ...
        (cross(UnitVecDetector,cross(UnitVecDetector-betaVec,betaDotVec))/c0 + ...
        (UnitVecDetector-betaVec)/(gamma^2*Distance)); % Velocity term
        MagneticField(Step,:) = 1/c0*cross(UnitVecDetector, ElectricField(Step,:));
    end
    FieldMagnitude(Step) = sqrt(dot(ElectricField(Step,:),ElectricField(Step,:)));
    DetectorTime(Step) = ParticleTime + Distance/c0;
else % Frequency-domain calculation using paraxial approximation
    PhiT = 2*pi*Frequency*(ParticleTime-ParticlePosition(3)/c0+(DetectorPos(k,1)-ParticlePosition(1))^2+ ...
    ((DetectorPos(k,2))^2)/(2*c0*(DetectorPos(k,3)-ParticlePosition(3))));
    FourierX(k,:) = FourierX(k,:) + cos(Angle)*deltat/Divider*c0.*exp(i*PhiT)/(DetectorPos(k,3)-ParticlePosition(3))* ...
    (beta*sin(Angle)-(DetectorPos(k,1)-ParticlePosition(1))/(DetectorPos(k,3)-ParticlePosition(3)));
    FourierY(k,:) = FourierY(k,:) + cos(Angle)*deltat/Divider*c0.*exp(i*PhiT)/(DetectorPos(k,3)-ParticlePosition(3))* ...
    (-DetectorPos(k,2)/(DetectorPos(k,3)-ParticlePosition(3)));
end

% Adapt divider if change of electric field magnitude is too fast in time-domain mode.
if (Step>1 && CalcMode==2)
    if (abs(FieldMagnitude(Step)-FieldMagnitude(Step-1)) > MaxFieldChange) && (Divider < MaxDivider)
        Divider = Divider * 2;
        continue;
    elseif (abs(FieldMagnitude(Step)-FieldMagnitude(Step-1)) < MaxFieldChange/2) && (Divider > 1)
        Divider = Divider / 2;
    end
end

% Track particle to next position and calculate total emitted energy
ParticleTime = ParticleTime + deltat/Divider;
if B~=0
    R = m0*c0/e0*gamma/B;
    deltaAngle = c0/R*deltat/Divider*beta;
    ParticlePosition = ParticlePosition + R*[(1-cos(deltaAngle))*cos(Angle)+sin(deltaAngle)*sin(Angle) 0 ...
    -(1-cos(deltaAngle))*sin(Angle)+sin(deltaAngle)*cos(Angle)];
    Angle = Angle + deltaAngle;
    IntEnergy = IntEnergy + e0^4*gamma^2*B^2/(6*pi*epsilon0*m0^2*c0)*deltat/Divider;
else
    ParticlePosition = ParticlePosition + c0*deltat*beta/Divider*[sin(Angle) 0 cos(Angle)];
end

Trajectory(Step,:) = [ParticlePosition(1) ParticlePosition(3)];

```

```

Step = Step + 1;
end % Loop over particle trajectory

if Step==MaxSteps && CalcMode~=2
    disp '*** Attention: Simulation stopped by exceeding maximum number of steps ! ***'
    return;
end
Step = Step - 1;

if CalcMode~=2
    fprintf(1,'Calculating Fourier spectrum...\r');
    FourierX(k,:) = FourierX(k,:) + 1/(2*pi*i)./Frequency.*(ElectricField(1:Step-1,1).*(exp(-2*pi*i*(DetectorTime(1:Step-1)).'*Frequency)).* ...
    (1-exp(-2*pi*i*(diff(DetectorTime(1:Step)).'*Frequency)))));
    FourierY(k,:) = FourierY(k,:) + 1/(2*pi*i)./Frequency.*(ElectricField(1:Step-1,2).*(exp(-2*pi*i*(DetectorTime(1:Step-1)).'*Frequency)).* ...
    (1-exp(-2*pi*i*(diff(DetectorTime(1:Step)).'*Frequency)))));
    FourierZ(k,:) = FourierZ(k,:) + 1/(2*pi*i)./Frequency.*(ElectricField(1:Step-1,3).*(exp(-2*pi*i*(DetectorTime(1:Step-1)).'*Frequency)).* ...
    (1-exp(-2*pi*i*(diff(DetectorTime(1:Step)).'*Frequency)))));
    if CalcMode==1
        FourierMagX(k,:) = FourierMagX(k,:) + 1/(2*pi*i)./Frequency.*(MagneticField(1:Step-1,1).'* ...
        *(exp(-2*pi*i*(DetectorTime(1:Step-1)).'*Frequency)).* (1-exp(-2*pi*i*(diff(DetectorTime(1:Step)).'*Frequency)))));
        FourierMagY(k,:) = FourierMagY(k,:) + 1/(2*pi*i)./Frequency.*(MagneticField(1:Step-1,2).'* ...
        *(exp(-2*pi*i*(DetectorTime(1:Step-1)).'*Frequency)).* (1-exp(-2*pi*i*(diff(DetectorTime(1:Step)).'*Frequency)))));
        FourierMagZ(k,:) = FourierMagZ(k,:) + 1/(2*pi*i)./Frequency.*(MagneticField(1:Step-1,3).'* ...
        *(exp(-2*pi*i*(DetectorTime(1:Step-1)).'*Frequency)).* (1-exp(-2*pi*i*(diff(DetectorTime(1:Step)).'*Frequency)))));
    end
end

end % Loop over mirror charges

if CalcMode==2
    FourierX(k,:) = -2*pi*i*Frequency*e0/c0^2.*FourierX(k,:)/(4*pi*epsilon0);
    FourierY(k,:) = -2*pi*i*Frequency*e0/c0^2.*FourierY(k,:)/(4*pi*epsilon0);
    Step = 2; % to avoid error from display commands below
else
    TotalEnergy(k) = epsilon0*c0*dot(FieldMagnitude(1:Step-1).^2,diff(DetectorTime(1:Step)));
    fprintf('Total energy in time domain: %.4g J/m^2\n', TotalEnergy(k));
end
if CalcMode==1
    S = cross([FourierX(k,:);FourierY(k,:);FourierZ(k,:)],conj([FourierMagX(k,:);FourierMagY(k,:);FourierMagZ(k,:)]));
    IntensityAcc(k,:) = 2*epsilon0*c0^2*sqrt(dot(real(S),real(S)));
else
    IntensityAcc(k,:) = 2*epsilon0*c0*(abs(FourierX(k,:)).^2+abs(FourierY(k,:)).^2+abs(FourierZ(k,:)).^2);
end

if length(Frequency)>1
    fprintf('Total energy in frequency domain: %.4g J/m^2\n', dot(IntensityAcc(k,1:length(Frequency)-1),diff(Frequency)));
end
fprintf('Total emitted energy by electron: %.4g J\n', IntEnergy);

end % Loop over detector positions

```

References

- [Coï79] R. Coïsson, *Angular-spectral distribution and polarization of synchrotron radiation from a 'short' magnet*, Phys. Rev. A **Vol. 20, No. 2**, 524 (1979)
- [Chu93] O.V. Chubar, N.V. Smolyakov, *Generation of intensive long-wavelength edge radiation in high-energy electron storage rings*, Proceedings of the 15th IEEE Particle Accelerator Conference, Washington D.C., 17-20 May 1993, pp. 1626-1628
- [Dohl98] M. Dohlus, T. Limberg, *Calculation of synchrotron radiation in the TTF-FEL bunch compressor magnet chicanes*, Nucl. Instr. Meth. **A 407**, 278 (1998)
- [Gel03] G. Geloni et al., *A method for ultrashort electron pulse-shape measurements using coherent synchrotron radiation*, DESY 03-031 (March 2003)
- [Gel05] G. Geloni et al., *Paraxial Green's function in synchrotron radiation theory*, DESY 05-032 (February 2005)
- [Gri06] O. Grimm, P. Schmüser, *Principles of coherent radiation diagnostics*, TESLA FEL 2006-03 (2006)
- [Sal97] E.L. Saldin et al., *On the coherent radiation of an electron bunch moving in an arc of a circle*, Nucl. Instr. Meth. **A 398**, 373 (1997)

- [Jack75] J. D. Jackson, *Classical Electrodynamics*, John Wiley & Sons, New York (1975)
- [Méot99] F. Méot, *A theory of low frequency far-field synchrotron radiation*, Part. Accel. **62**, 215 (1999)
- [Pae08] A. Paech, *Evaluation numerischer Methoden zur Berechnung von Synchrotronstrahlung am ersten Bunchkompressor des Freie-Elektronen-Lasers FLASH*, PhD thesis Technische Universität Darmstadt, February 2008
- [Nod54] J.S. Nodvick, D.S. Saxon, *Suppression of coherent radiation by electrons in a synchrotron*, Phys. Rev. **96**, 180 (1954)
- [Bos02] R.A. Bosch, *Shielding of infrared edge and synchrotron radiation*, Nucl. Instr. Meth. **A 482**, 789 (2002)
- [War90] R. L. Warnock, *Shielded coherent synchrotron radiation and its effect on very short bunches*, SLAC-PUB 5375 (November 1990)
- [Stu04] F. Stulle, *A Bunch Compressor for small Emittances and high Peak Currents at the VUV Free-Electron Laser*, PhD thesis Universität Hamburg, August 2004